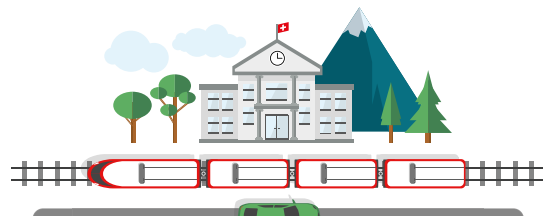


ALMA MATER STUDIORUM · UNIVERSITY OF BOLOGNA

Flatland Challenge



FLATLAND

Deep learning course final project

Leonardo Calbi (leonardo.calbi@studio.unibo.it)
Alessio Falai (alessio.falai@studio.unibo.it)

January 14, 2021

Contents

1	Introduction	5
2	Background	6
3	Environment	11
3.1	Railway encoding	11
3.2	Predictions	15
3.2.1	Shortest and deviation paths	15
3.3	Real decisions and choices	16
3.3.1	Real decisions	16
3.3.2	Choices	16
3.4	Observations	17
3.4.1	Tree	19
3.4.2	Binary tree	21
3.4.3	FOV	23
3.4.4	Normalization	24
4	Reinforcement learning setting	26
4.1	Rewards and shaping	28
4.2	Action selection	29
4.2.1	ϵ -greedy	29
4.2.2	Boltzmann	30
4.3	Action masking	30
5	DQN	32
5.1	Experience replay	33
5.2	Improvements	34
5.2.1	Double	34
5.2.2	Dueling	34
5.2.3	Gradient noise reduction	35
5.2.4	Bellman operators	36
6	GNN	38
6.1	Integrating GNNs in DQNs	40
6.2	Architectures	41
6.2.1	Entire graph embeddings	41
6.2.2	Multi-agent graph embeddings	42
7	Results	44
8	Conclusions	57

List of Figures

2.1	Different railcell types	6
2.2	Agents and targets	7
2.3	An example of a railway environment	7
2.4	Transition matrix and bitmap of a deadend	8
2.5	Examples of deadlocks	10
3.1	Different railway encodings of a 32×16 map	13
3.2	Grid and COJG comparison in a sparse 128×64 map	14
3.3	Default observators	19
3.4	Tree observator	20
3.5	Shortest path and one deviation path channels extracted from a 3×3 FOV in a 4×5 toy environment	24
4.1	Single agent RL scenario	26
4.2	Agent with a subset of legal actions	31
5.1	Simple DQN example with FC layers	33
5.2	Dueling DQN architecture	35
6.1	Input graph with GNN aggregation (example taken from [12])	39
6.2	Multi-agent graph embeddings architecture (image taken from [14])	42
7.1	Binary tree training metrics on the medium environment	48
7.2	Standard vs. softmax Bellman training metrics	51
7.3	Action selectors comparison training metrics	53

List of Tables

3.1	Grid, COG, COJG comparison in a 32×16 map	12
3.2	Grid, COG, COJG comparison in a 128×64 map	12
3.3	Tree vs. binary tree efficiency in a 48×27 map, with $d = 7$	23
7.1	Test environments settings	44
7.2	Hyperparameters description	46
7.3	Binary tree hyperparameters, trained on medium environment	47
7.4	Binary tree results, tested on medium environment	49
7.5	Binary tree results, tested on big environment	49
7.6	Standard vs. softmax Bellman hyperparameters, trained on medium environment	50
7.7	Standard vs. softmax Bellman results, tested on medium environment	50
7.8	Action selectors comparison results, tested on medium environment	52
7.9	Single-agent entire graph embeddings hyperparameters, trained on medium environment	54
7.10	Single-agent entire graph embeddings vs. random baseline results, tested on medium environment	54
7.11	Multi-agent graph embeddings hyperparameters, trained on medium environment	55
7.12	Multi-agent graph embeddings results, tested on medium environment	55

Foreword

The Flatland challenge is a competition organized by Alcrowd [1] with the help of SBB (Swiss Federal Railways) to foster innovation with what regards the scheduling of trains trajectories in a railway environment.

As reported on the official challenge website, SBB operates the densest mixed railway traffic in the world and maintains the biggest railway infrastructure in Switzerland: today, as of 2021, there are more than 10 000 trains running each day, being routed over 13 000 switches and controlled by more than 32 000 signals.

The Flatland challenge aims to address the vehicle rescheduling problem by providing a simplistic grid world environment and allowing for diverse solution approaches. In particular, the first edition of the challenge was hosted during 2019 and the submitted solutions were mainly based on OR (Operation Research) methodologies, while the second edition of the competition, i.e. the NeurIPS 2020 edition, had the goal of favoring the implementation of RL (Reinforcement Learning) based solutions.

1 Introduction

At the core of this challenge lies the general vehicle rescheduling problem (VRSP) proposed by Li, Mirchandani, and Borenstein in 2007 [13]:

The vehicle rescheduling problem (VRSP) arises when a previously assigned trip is disrupted. A traffic accident, a medical emergency, or a breakdown of a vehicle are examples of possible disruptions that demand the rescheduling of vehicle trips. The VRSP can be approached as a dynamic version of the classical vehicle scheduling problem (VSP) where assignments are generated dynamically.

The problem is formulated as a 2D grid environment with restricted transitions between neighboring cells to represent railway networks. On the 2D grid, multiple agents with different objectives must collaborate to maximize the global reward.

The overall goal is to make all agents (trains) arrive at their target destination with a minimal travel time. In other words, we want to minimize the time steps (or wait time) that it takes for each agent in the group to reach its destination.

2 Background

Railway

As already pointed out, the Flatland environment is represented as a 2D grid of dimension $W \times H$ and each cell in the grid can be one of many different types. The different types of cells can belong to the following categories: `rail` and `empty`.

The `rail` cells are the most intricate of the two, in that there exists different types of them. In particular, figure 2.1 shows examples of possible `rail` cells that can be used to build up a railway environment in Flatland. Other than the ones shown in figure 2.1 there are also diamond crossings (i.e. two orthogonal straight rails crossing each other), single slip switches (i.e. the same as double slip switches but with a single choice) and symmetrical switches (which are special kinds of switches that bifurcate to a left and right branch). Moreover, every `rail` cell can be rotated by 90° and mirrored along both axis, to allow more combinations between them to be made, in order to guarantee a greater degree of diversity between different railways.

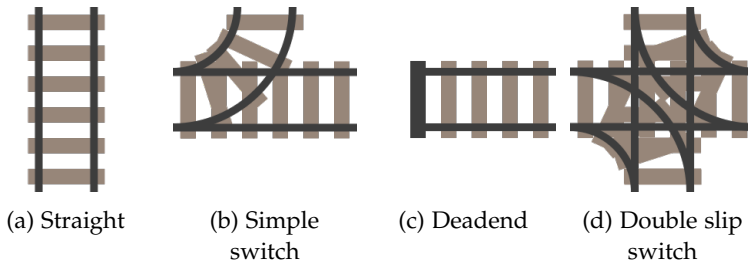


Figure 2.1: Different `rail` cell types

Moreover, `rail` cells can be occupied by the following entities (the ones shown in figure 2.2):

- Agent: one `rail` cell can be seen as a resource with availability equal to one, so that in each time step only one agent can occupy it
- Target: each target is statically assigned to one `rail` cell. Target cells represent the destination of one or more agents (different agents could have the same target). Moreover, the number of possible targets present in the environment is clearly limited by the number of agents

An important fact about the different types of `rail` cells is that only switches require an agent to make a choice. In Flatland (like in reality) a maximum of two options is available. There does not exist a switch with three or more options.

Finally, every cell that is not `rail` is `empty` and neither targets nor agents can



(a) Agent (b) Target

Figure 2.2: Agents and targets

fill it up. As shown in figure 2.3, it is interesting to notice that Flatland is a very sparse environment, meaning that there are a lot more empty cells than rail ones: because of this, representing the environment as a simple dense matrix could lead to overheads and efficiency issues, especially when dealing with relatively big environments.

In the end, the only cell types that we care about are the `rail` ones: the empty ones are useful only for visualization purposes. Because of this, we could think of representing the environment as a sparse matrix or as a graph containing only `rail` cells or a subset of them (we will address this issue in section 3.1).

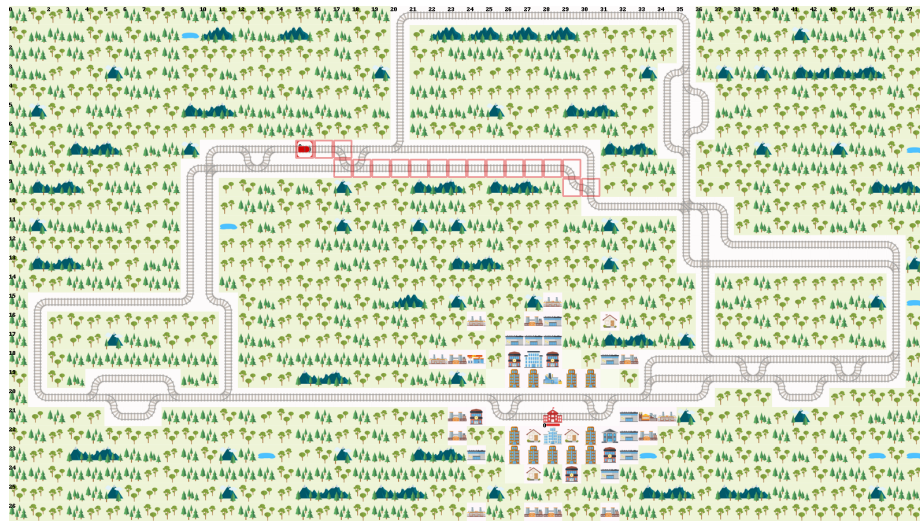


Figure 2.3: An example of a railway environment

Transitions

An agent in the Flatland environment is a train that starts from a random rail cell in the map and has to arrive to its assigned target in the minimum number of steps. To do so, the agent can only occupy rail cells.

To move from a cell to another one the agent has to make a choice and, de-

pending on the cell type that they are on and on the connections between cells, an agent can transition from cell i , when looking towards direction d_i , to cell j , looking towards direction d_j , if and only if $T_i(d_i, d_j) = 1$, where T_i is the transition matrix associated to cell i , s.t. $T_i(d_i, d_j) = 0$ means that the transition from cell i , direction d_i to cell j , direction d_j is forbidden (likewise $T_i(d_i, d_j) = 1$ means that the transition is allowed). Directions d_* are represented as the 4 cardinal directions, i.e. North, East, South and West (N, E, S, W), so that each transition matrix T_* can be characterized as a 4×4 binary matrix. For example, a deadend cell like the one reported in figure 2.1c would have a transition matrix like the one shown in figure 2.4.

$$\begin{array}{l}
 \begin{array}{cccc} N & E & S & W \end{array} \\
 \begin{array}{l} N \\ E \\ S \\ W \end{array} \left(\begin{array}{cccc} 0 & 0 & 0 & 0 \\ 0 & 0 & 0 & 1 \\ 0 & 0 & 0 & 0 \\ 0 & 0 & 0 & 0 \end{array} \right) \xrightarrow{\text{to bitmap}} 0000\ 0001\ 0000\ 0000
 \end{array}$$

Figure 2.4: Transition matrix and bitmap of a deadend

As we can observe, only one entry in the matrix has value 1, meaning that only one transition is possible, i.e. the one s.t. the agent enters heading East and exits heading West.

In the Flatland library, a transition matrix is represented by a bitmap, which can be seen as a linearization by rows of the reported matrix (the mapping between the transition matrix of the deadend cell 2.1c and its bitmap is again shown in figure 2.4). In this way, by simply counting the number of true values in the bitmap, we can understand the type of rail cell that we are examining (e.g. only one true value indicates a deadend, while exactly two true values indicate a straight rail).

Actions

Flatland has a discrete action space, meaning that only 5 possibilities have to be considered at each transition. In particular, Flatland uses the following convention:

1. MOVE_FORWARD: the agent maintains the current movement direction, if possible (i.e. if it was heading North, it will continue heading North)
2. MOVE_LEFT: if the agent is at a switch with a transition to its left, the agent will choose the left path, otherwise the action has no effect (e.g. if the agent was heading North, it will be directed towards East)
3. MOVE_RIGHT: if the agent is at a switch with a transition to its right, the agent will choose the right path, otherwise the action has no effect (e.g. if the agent was heading North, it will be directed towards West)
4. STOP_MOVING: the agent remains in the same cell

5. DO NOTHING: the agent performs the same action as the last time step

Usually, only a handful of the reported actions can be performed on a given cell, meaning that most of the times the actual number of choices is much less than 5 (we will address this issue in section 3.3).

Complications

The main complications of the Flatland challenge are given by speed profiles, conflicts and malfunctions. In particular, about speed profiles, each and every agent could have a different velocity. The standard speed (and the maximum one) is 1, which means that the agent crosses one cell in one time step. Speeds can have values in range $(0, 1]$: if an agent has speed s , it means that it needs $\lceil \frac{1}{s} \rceil$ time steps to transition from one cell to the next one.

Speeds are assigned to agents based on a custom probability mass function, so that $P(S = s)$ represents the probability that the speed S of an agent is equal to s . For example, we could have the following pmf (representing a uniform distribution over values $\{\frac{1}{4}, \frac{1}{3}, \frac{1}{2}, 1\}$):

$$\begin{cases} P(S = s) = 0.25 & \text{if } s \in \{\frac{1}{4}, \frac{1}{3}, \frac{1}{2}, 1\} \\ P(S = s) = 0 & \text{otherwise} \end{cases}$$

Clearly, the speed factor is a critical one to observe when trying to minimize the total number of time steps in a multi-agent scenario: for example, different agents have to understand that faster ones should go first if a decision has to be made. This is because we would like to avoid bottlenecks of any kind inside the railway network and slower agents can definitely become an issue in an environment with relatively long sequences of straight rails.

About the second complications, i.e. malfunctions, agents can experience defects or failures which do not let them go on in their path towards the target. A malfunction in the Flatland environment is modeled by a Poisson distribution $1 - P_\lambda(n = 0) = 1 - \frac{\lambda^n}{n!} \cdot e^{-\lambda} = 1 - e^{-\lambda}$, where $\lambda \in (0, 1]$ is the malfunction rate s.t. $\frac{1}{\lambda}$ represents the mean frequency of occurrence of malfunctioning events. For example, if malfunctions are to be expected once every 80 time steps for an agent, then $\lambda = \frac{1}{80} = 0.0125$ and the probability of a malfunction in each time step is equal to $1 - e^{-0.0125} = 0.01$, while if malfunctions are more rare (e.g. once every 200 time steps), then we would have a probability value of $1 - e^{-0.005} = 0.004$. Once an agent is malfunctioning, it stays so for a random number of time steps, bounded by parameters indicating the minimum and maximum duration of a malfunction period.

Again, the malfunction factor is critical, in that it could prevent one or more agents from reaching their targets in the minimum number of time steps. In this way, transitions in the environment become stochastic, thus leading to a slower and much more difficult optimization procedure.

About the third complication, i.e. conflicts, we can define it as a state in which agents cannot perform any action, because they are "blocked" by one or more

neighboring agents. Different conflicting situations can arise in practice, where the most basic one is given by two agents heading in different directions in a sequence of straight rails (see figure 2.5a): this situation can in turn cause other deadlocks to happen, as shown in figure 2.5b.

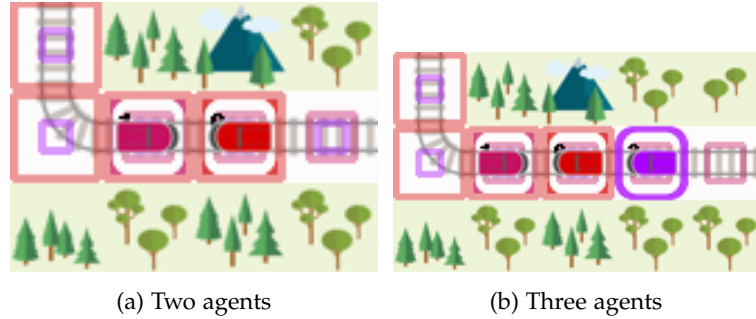


Figure 2.5: Examples of deadlocks

A full deadlock situation is a state in which every agent is in deadlock: in that case, no agent would be able to arrive at its target. These blocking situations are one of the most intricate and complex factors that should be addressed when designed autonomous agents in the Flatland environment, since they are quite frequent (and they get more frequent as the number of agents increases and the dimension of the grid decreases) and have disastrous consequences (at least in a real-world scenario).

Differently from malfunctions, deadlocks totally prevent agents from reaching their destination: when a malfunction occurs, agents that could previously reach their targets will still be able to reach them once the malfunction period is over, while when a conflict occurs, at least two agents will never arrive at their targets.

3 Environment

In this chapter we are going to explore better ways to encode the Flatland environment and how agents can interact with these representations.

3.1 Railway encoding

As already described in chapter 2, the default Flatland representation was not built with the goal of efficiency in mind, since it stores each and every cell of the 2D grid, while only `rail` cells are the ones that are actually used by agents. An alternative and more efficient representation could be to use some kind of sparse matrix implementation, where `empty` cells are not stored at all, but this would only be beneficial from the point of view of memory occupancy, while the usage of more specific data structures could also improve other aspects, like the computation of shortest paths from the agent's position to its target.

In this project, we decided to rely on a graph structure. In particular, we were inspired by the great work described in [10] where the author presents the so called Cell Orientation Graph (COG), in which nodes represent cells in the 2D grid as a triple (x, y, d) , where (x, y) are the coordinates in the grid (origin in the top-left corner with x-axis looking right and y-axis looking down) and d is one of the four cardinal directions (representing the direction of entrance in the cell). In this way, one `rail` cell is represented by at most 4 nodes in the graph: this could seem like a major drawback, but in practice we can observe that the number of nodes is roughly equivalent to the number of cells in the corresponding grid, since we got rid of the `empty` ones.

Instead, edges in the graph are directed and represent legal transitions, so that no transition matrix or bitmap has to be stored in each node: it is simply encoded in the topology of the network. Moreover, the usage of directed edges greatly simplifies the computation of paths between nodes in the graph.

In order to further simplify the representation of the Flatland environment, we decided to entirely delete nodes which represented straight rails (with the exception of keeping straight rails containing targets and deadends). In this way, what we end up with is something that could be defined a Cell Orientation Junction Graph (COJG), since the remaining nodes are the ones in which an agent either has to make a decision or finishes its trip.

Because of the deletion of almost all nodes associated to straight rails, edges actually represent a connection between an interesting cell and another one (e.g. they link a junction to a target or a junction to a second junction). In order to maintain the same topology as before, the number of deleted straight rails between each pair of interesting nodes is used as the weight of the edge

connecting them, so that the computation of shortest paths can automatically take that into account.

Figure 3.1 shows the comparison, in terms of visual representations, of the standard grid environment and both COG and COJG graphs, in a 32×16 map. In table 3.1 we show the improvements that can be gained by leveraging the usage of the Cell Orientation Graph, and in particular of its modified version, i.e. the Cell Orientation Junction Graph, by computing the number of nodes, edges and empty cells in each representation, in the same 32×16 map of figure 3.1.

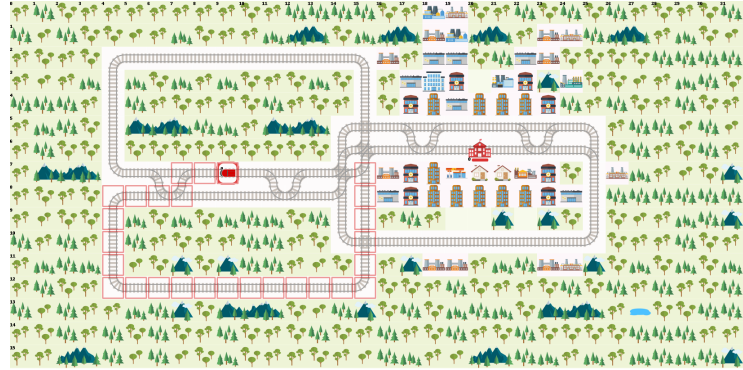
	Nodes	Edges	Empty
Grid	512	-	413
COG	226	254	0
COJG	78	106	0

Table 3.1: Grid, COG, COJG comparison in a 32×16 map

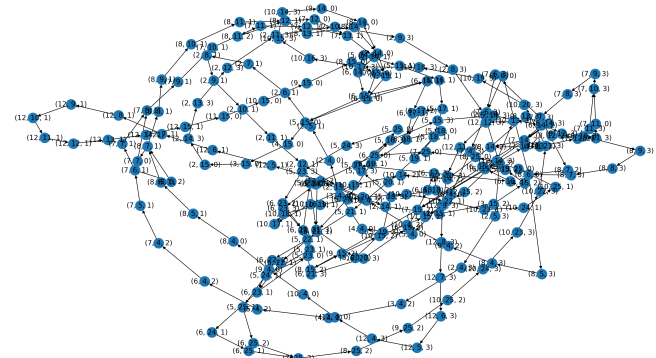
Since a 32×16 map is too small to observe big improvements, in figure 3.2 we also report another example of a sparse grid environment of dimension 128×64 and we compare it with its encodings in table 3.2.

	Nodes	Edges	Empty
Grid	8192	-	7732
COG	1050	1096	0
COJG	136	182	0

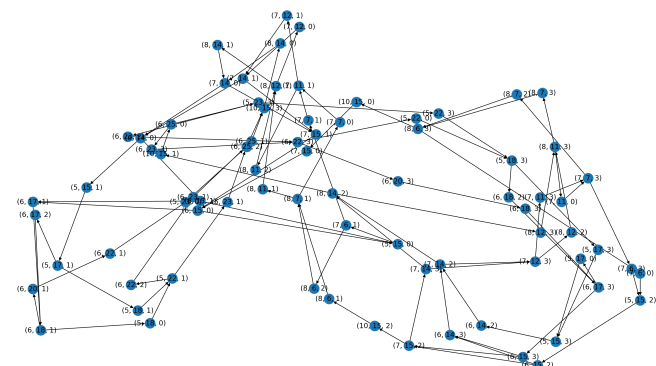
Table 3.2: Grid, COG, COJG comparison in a 128×64 map



(a) Grid

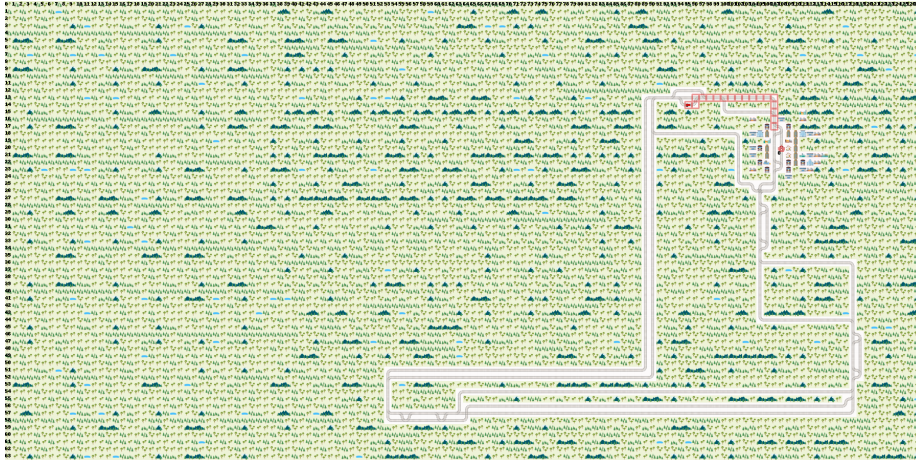


(b) COG

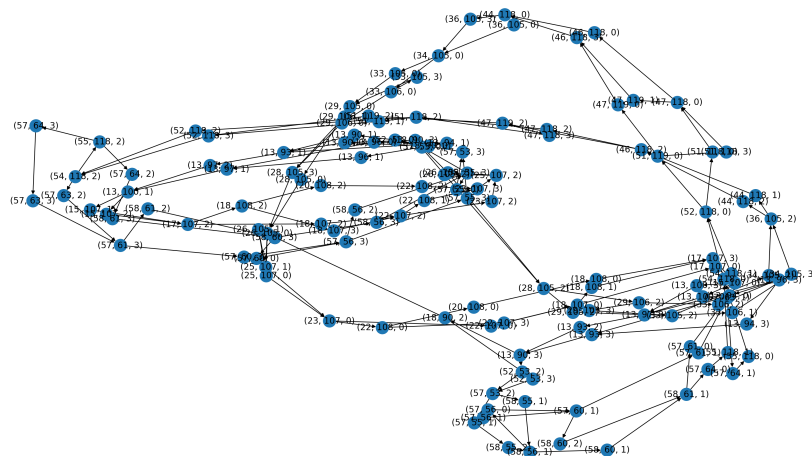


(c) COJG

Figure 3.1: Different railway encodings of a 32×16 map



(a) Grid



(b) COJG

Figure 3.2: Grid and COJG comparison in a sparse 128×64 map

3.2 Predictions

As reported in Flatland official FAQs, because railway traffic is limited to rails, many decisions that an agent has to take need to consider future situations and detect upcoming conflicts ahead of time. Therefore, Flatland provides the possibility of predictors that estimate where agents should be in the future. The stock predictor simply assumes that each agent travels along its shortest path.

3.2.1 Shortest and deviation paths

One of the key advantages of COJG is that it enables us to apply standard shortest path algorithms on directed weighted graphs without any kind of overhead. In particular, we decided to use Dijkstra's algorithm since we do not have negatively weighted edges (in that case, Dijkstra's algorithm could get stuck in a cycle containing at least one edge with negative weight, since it may cycle an infinite number of times and sometimes go down with the total cost as much as it likes).

To build our predictor, we took inspiration from the standard one given by the Flatland library as a baseline, which computes shortest paths directly on the 2D grid representation. Our predictor instead takes into account two possibilities: an agent either follows its shortest path or deviates from it. The computation of shortest paths is incremental, meaning that once it is done it only gets updated (i.e. the first node is removed). The only event that causes a re-computation of the shortest path is when the agent makes a choice that does not follow the stored path.

Deviation paths are instead computed on the fly and they represent alternatives from each node of the shortest path. The computation of deviation path i , given the shortest path $n_1, \dots, n_i, n_{i+1}, \dots, n_d$, is simply another call to the Dijkstra's routine, where edge (n_i, n_{i+1}) is forbidden. In this example, d represents the maximum depth of both shortest and deviation paths.

In this way, the prediction becomes a list of paths, where the first one is the shortest path, composed by at most d nodes, and the following ones are m deviation paths, still composed by at most d nodes. When an agent is relatively close to its target (i.e. less than d nodes away from it), the actual path could have a dimension which is less than d : to avoid troubles when dealing with dynamically sized vectors, paths are padded to the full depth with special symbols.

In case an agent cannot reach its target anymore, the prediction only comprises a path of two nodes, i.e. the agent's position and the next node in the COJG graph. This mini-path is stored because predictions are used to compute possible deadlocks and, even if an agent cannot arrive at its target anymore, it is still present in the railway environment and it could be a possible source of conflicts.

3.3 Real decisions and choices

3.3.1 Real decisions

As already hinted in the previous sections, Flatland railway environments are structured in such a way that most of them are composed by long sequences of straight rails, where an agent does not have to commit to any thoughtful choice, but it simply has to follow the path on which it is positioned. The agent is instead required to make a decision in two simple cases: whenever it reaches a fork, i.e. a cell that has more than one successor, or immediately before a join, i.e. before entering another path that crosses its next cell.

Following the reasoning described in [10], we categorize as real decisions those times in which an agent has to select an action when it is positioned in a fork, before a join or in a combination of the two cases. An agent in a fork has to decide on which branch to go next (and ideally, it should not choose to stop on that cell), while an agent before a join has to decide if it wants to stop (maybe to let another agent pass through the join cell) or continue moving.

This idea of introducing real decisions in the Flatland environment greatly reduces the number of calls to the model that is tasked to map states to actions, since the number of real decisions to take is much lower than the number of default actions that one has to provide in the standard framework. In particular, the default number of actions to select is equal to the number of steps that the agent performs in the environment, while the number of real decisions to take is entirely disentangled from the steps parameter, since it is completely dependent on the structure of the environment (e.g. sparser railways tend to have less real decisions w.r.t. denser ones, given the same grid size).

The concept of real decisions leads to a modification in the structure of the COJG graph reported in section 3.1, so that both types of decisions are encoded as nodes. In particular, COJG is missing most nodes related to cells before a join, since they are usually part of straight rails. Currently, our implementation patches the COJG graph, but a cleaner choice would be to actually add the before join nodes from the start of the building process, which could be something to try for future improvements.

3.3.2 Choices

Further analysis related to decisions, again presented in [10], shows a smart action space reduction that could be beneficial to reinforcement learning models. In particular, Flatland uses a discrete action space composed of 5 actions, which can be reduced to a total of 3. From now on, we will refer to elements of this new action space as "choices".

Choices are mapped in such a way that they correspond to the left-most and right-most directions available to the agent at each time-step. In this way, our model only has to predict whether the agent has to follow the track to its left or the track to its right or simply stop. After a choice is selected, it is

mapped back to the initial action space by looking at the type of cell the agent is currently on, to ensure compatibility with the Flatland environment.

The new action space is composed by the choices CHOICE_LEFT, CHOICE_RIGHT and STOP.

So, we have to specify two different mappings, the forward and the backward one. The action to choice mapping works as follows:

1. If the selected action is MOVE_LEFT and that action is legal from the current cell of the agent, then return CHOICE_LEFT
2. If the selected action is MOVE_RIGHT and that action is legal from the current cell of the agent, then
 - (a) If only MOVE_RIGHT can be performed, then CHOICE_LEFT is returned
 - (b) Otherwise, CHOICE_RIGHT is returned
3. If the selected action is MOVE_FORWARD and that action is legal from the current cell of the agent, then
 - (a) If MOVE_LEFT can be performed, then CHOICE_RIGHT is returned
 - (b) Otherwise, if MOVE_RIGHT can be performed, then CHOICE_LEFT is returned
 - (c) Otherwise, the last resort is CHOICE_LEFT
4. If STOP_MOVING, we have a one-to-one mapping with the STOP choice, so that the agent decides to stand still

Instead, the choice to action mapping works as follows:

1. If CHOICE_LEFT, then priorities are MOVE_LEFT, MOVE_FORWARD, MOVE_RIGHT
2. If CHOICE_RIGHT, then priorities are MOVE_RIGHT, MOVE_FORWARD
3. If STOP, then the only possible outcome is STOP_MOVING
4. Otherwise, last resort is DO NOTHING

In the previous bullet points, the word "priority" represents the sequential way in which actions should be selected. For example, if a CHOICE_RIGHT has to be mapped back and MOVE_RIGHT is a legal action from the current cell of the agent, then that action would be selected, otherwise MOVE_FORWARD would be chosen (again, if legal).

3.4 Observations

An observation is a representation of the environment in a particular state. Ideally, this snapshot should be rich enough to convey the right amount of information (so as to distinguish between different configurations), but also small enough that it would be efficient to compute at any given time-step. An observation should also be able to integrate information from local (in our case a train) and global (in our case the grid and all the agents) perspectives.

Flatland provides different observers out of the box (the ones roughly depicted in figure 3.3). In particular, the implemented global observation is composed of the following elements:

- Transition map tensor with shape $(h, w, 16)$, assuming 16 bits encoding of transitions
- A tensor with shape $(h, w, 2)$, containing the position of the given agent's target in the first channel and the positions of the other agents' targets in the second channel (flag only, no counter)
- A tensor of shape $(h, w, 5)$ with the following channels:
 1. Agent position and direction
 2. Other agents positions and direction
 3. Agents malfunctions
 4. Agents fractional speeds
 5. Number of other agents ready to depart

The implemented local observation should instead gather information of the rail environment around the given agent. This observation is composed of the following elements:

- Transition map tensor of the local environment around the given agent, with shape $(v_h, 2 \cdot v_w + 1, 16)$, assuming 16 bits encoding of transitions
- A tensor with shape $(v_h, 2 \cdot v_w + 1, 2)$ containing the target position of the given agent (if in the agent's vision range) in the first channel and the positions of the other agents' targets (again, if in the agent's vision range) in the second channel
- A tensor $(v_h, 2 \cdot v_w + 1, 4)$ containing the one-hot encoding of directions of the other agents at their position coordinates (if in the agent's vision range)
- A 4 elements array with a one-hot encoding of the current direction of the given agent

Here, the parameters v_w and v_h define the rectangular view of the agent (of dimension $(2 \cdot v_w + 1) \times v_h$) around its position. One thing to notice about the standard local observation is that it does not contain any clues about the target location, if it's out of range: thus, navigation on maps where the radius of the observation does not guarantee a visible target at all times will become very difficult.

Moreover, Flatland discourages the use of both the given global and local observations, since the first one does not seem to encode enough information to be effective in a multi-agent scenario, while the second one is simply deprecated in the newest version of their Python library, which makes it practically useless. Because of this, more advanced observations must be used in order to

achieve good results on a wide range of environments. In particular, in the following sections we will take a look at another observation present in Flatland library, i.e. the tree observation, and we will use it as the starting point to build our custom binary tree observation, which also integrates all the knowledge and findings that we described in the previous chapters.

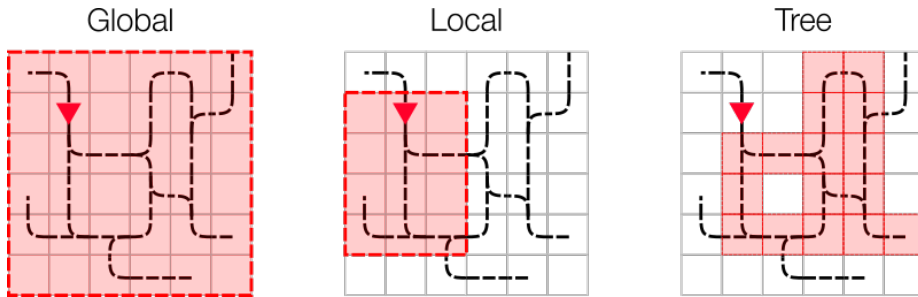


Figure 3.3: Default observers

3.4.1 Tree

The tree observation is the last one provided out of the box in the Flatland package and it's definitely the most effective overall (w.r.t. the already mentioned global and local ones). This observator builds a tree with arity 4, s.t. the children of a node always follow a left, forward, right and backward ordering. In particular, a node in the tree represents a deadend, a switch, a target destination or a blank (meaning that no information is carried by that specific node). The children of a node represent its successor nodes when following the left/right/forward branch on a switch or the backward one on a deadend. The mentioned movements are sorted relative to the current orientation of the agent, rather than using standard transition directions (i.e. the four cardinal directions). Whenever a node does not have one of the mentioned successors, that branch becomes useless and gets filled with padding values.

Figure 3.4 shows a mapping between a state and the corresponding tree observation, from the point of view of the agent represented by the red triangle. The colors in the figure illustrate what branch the cell belongs to (red means left, pink means forward, green means right and blue means backward). If there are multiple colors in a cell, then this cell will be present multiple times in the tree. The symbols in the figure have instead the following meaning:

- Cross: no branch was built, i.e. the parent does not have a valid transition to represent the child
- No children: the node is a terminal node (i.e. a deadend, a cell without possible transitions or a leaf of the tree, indicating that the maximum depth was reached)
- Circle: a node filled with information

Whenever a node is valid, it will be packed with the following features:

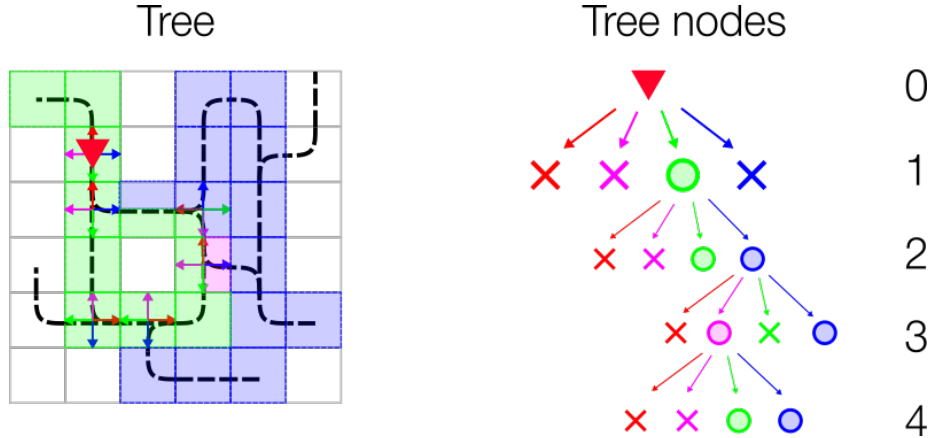


Figure 3.4: Tree observator

1. If the target of the given agent lies on the explored branch, the current distance from the given agent (in number of cells) is stored
2. If another agent's target is detected, the distance in number of cells from the given agent's current location is stored
3. If another agent is detected, the distance in number of cells from the given agent's position is stored
4. If another agent predicts to pass along this cell at the same time as the given agent, the distance (in number of cells) from the given agent's position is stored
5. If an unusable switch is detected for the given agent, the current distance (in number of cells) from the given agent's position is stored
6. Distance in number of cells to the next branching
7. Minimum distance from the node to the given agent's target, considering the current direction of the agent
8. Number of agents present in the same direction as the given agent
9. Number of agents present in the opposite direction as the given agent
10. Number of time steps that the given agent remains blocked, if a malfunctioning agent is encountered
11. Slowest observed speed of agents in the same direction as the given agent
12. Number of agents ready to depart, but not yet active

One key issue about the described tree observation is related to both time and memory efficiency. In particular, we mentioned a maximum depth parameter that controls how far the observation should reach, in terms of consecutive switches, targets and deadends visited. Clearly, since each node has 4 children

and the output of the observator should be consistent, running it requires to build a complete tree, which we know to have a number of nodes equal to:

$$n = \sum_{i=0}^{d-1} a^i,$$

where d is the height of the tree (i.e. our maximum depth) and the arity a is equal to 4. Just to make a quick example, if $d = 7$ then $n = 4^0 + 4^1 + 4^2 + 4^3 + 4^4 + 4^5 + 4^6 = 5461$. In this way, in the worst case, for each time-step we would have to examine $t \cdot n$ nodes, where t is the number of trains, since one observation is needed for each agent. Following the previous example, in a scenario with $t = 10$ agents and a tree observation with depth $d = 7$, the reported features should be computed for each of the $5641 \cdot 10 = 56\,410$ analyzed nodes at every time-step.

3.4.2 Binary tree

In order to exploit what we've built so far and have an hopefully more efficient computation of each observation, a new observator was created, starting from the same notions described in section 3.4.1.

In particular, our observator builds a feature tensor of shape $(m+1, d, f)$, where $m+1$ is the number of paths returned by the predictor introduced in 3.2.1, d is the maximum number of hops in the COJG graph to consider and f is the total amount of features for each node. This tensor contains the features of the nodes in the shortest path as the first row and the features of the nodes in the deviation paths (which are exactly m) as the following rows.

Each node has the following features:

1. Number of agents (going in the same direction as the one of the given agent) identified in the subpath from the root up to each node in the path
2. Number of agents (going in a direction different from the one of the given agent) identified in the subpath from the root up to each node in the path
3. Number of malfunctioning agents (going in the same direction as the one of the given agent) identified in the subpath from the root up to each node in the path
4. Number of malfunctioning agents (going in a direction different from the one of the given agent) identified in the subpath from the root up to each node in the path
5. Minimum distances from an agent to other agents (going in the same direction as the one of the given agent), in each edge of the path
6. Minimum distances from an agent to other agents (going in a direction different from the one of the given agent), in each edge of the path

7. Maximum number of malfunctioning turns of other agents (going in the same direction as the one of the given agent), in each edge of the path
8. Maximum number of malfunctioning turns of other agents (going in a direction different from the one of the given agent), in each edge of the path
9. Distances from the target, from each node in the path
10. Path weights (in number of turns) to reach the given node from the root one
11. Number of agents using the node to reach their target in the shortest path
12. Number of agents in deadlock in the previous path, assuming that all the other agents follow their shortest path
13. How many turns before a possible deadlock
14. If the node is a fork or not
15. How many turns the current agent has been repeatedly selecting the stop action

Initially, we tried to use the feature tensor as our final observation. In particular, we linearized it as a $m \times d \times f$ vector and fed it into one of the neural models that will be described in the next chapters. In this way, the model was not converging to reasonable solutions, since we were ignoring consistency, meaning that in neural models each and every input neuron should always represent the same measure. Instead, since our feature tensor was built by simply considering paths in the environment, one specific node could have represented either the left or the right branch being taken from the previous node, in different runs. This was definitely confusing the agents, so that no convergence was reached.

Because of this, we resorted to the same idea that was presented in [3.4.1](#), but, thanks to the new action space introduced in [3.3.2](#), we were able to shape the feature tensor like a binary tree (i.e. a tree with arity $a = 2$), where branches identify choices, i.e. CHOICE_LEFT or CHOICE_RIGHT. One key difference that our custom binary tree has w.r.t. the standard tree observation is the injection of prior knowledge: this is done by filling in values of features that are only related to nodes present either in the shortest or in one of the deviation paths. In this way, the binary tree contains only information about paths that could lead to the agent's target, by completely disregarding the ones that could not.

Since the resulting tree has half the arity of the one given by Flatland and we still need a complete tree for consistency reasons, let's consider again the example reported in [3.4.1](#) to roughly check for efficiency improvements, where a maximum depth of $d = 7$ was chosen, with $t = 10$ trains. Our complete binary tree would have $n = 2^0 + 2^1 + 2^2 + 2^3 + 2^4 + 2^5 + 2^6 = 127$ nodes (compared to 5641) and the number of total nodes for which features would have to

be computed at each time-step would be around $127 \cdot 10 = 1270$ (compared to 56410). Moreover, the reported number (1270) is an upper bound on the actual number of nodes that should be analyzed, since different time-steps will require different agents to compute an observation, i.e. only those agents that find themselves in a real decision cell.

To sum up efficiency improvements, each feature is built from scratch, by leveraging the performance gains obtained with the COJG graph. Moreover, the observation needs to be computed only when the agent faces a real decision (as described in section 3.3.1), since in every other scenario the action that the agent should take is implicit. By combining this with the much lower size of the tree (compared to Flatland’s implementation), we are able to compute more observations with less resources overall. Table 3.3 shows a comparison of the standard tree observation and our custom binary tree one, in terms of both running times and memory occupancy for a single observation. As we can see, the binary tree observation is around 6 times faster on average and occupies 30 times less memory on average than the tree one.

	Time (s)		Memory (MB)	
	Avg	Std	Avg	Std
Tree	0.1978	0.0199	0.4806	0.0
Binary tree	0.0335	0.0124	0.0153	0.0

Table 3.3: Tree vs. binary tree efficiency in a 48×27 map, with $d = 7$

3.4.3 FOV

Starting from the already provided, but deprecated, local observation present in the Flatland package, the FOV observator provides a Field Of View around the position of a given agent. In particular, the FOV observator builds a feature map of size $(7 + m, d, d)$, where m is the maximum number of deviation paths (the ones described in 3.2.1) and d is the side of the square view associated to each agent.

Since we want to emphasize the agent related to the observation, d should be an odd number, so that the agent’s position can always be represented by the central cell $(\lfloor d/2 \rfloor, \lfloor d/2 \rfloor)$ of the FOV.

About individual features reported in the agent’s FOV channels:

1. Cell type: empty cell 0 is encoded as -1 , while cell types 1 to 10 are encoded as-is
2. Cell orientation: 0, 90, 180, 270 degrees are encoded as 0, 1, 2, 3
3. Shortest path: distance from target for cells in the shortest path and -1 otherwise
4. Positions: other agents are represented by their current direction
5. Targets: 1 for the agent target, 0 for other agent’s targets, -1 otherwise

6. Malfunctions: number of remaining malfunctioning turns for all the agents in the FOV
7. Speeds: fractional speeds of all the agents in the FOV
8. Deviation paths: one channel for each deviation path, following the same encoding of the shortest path

Figure 3.5 shows an example of two channels taken from a 3×3 FOV in a 4×5 toy environment, where the first channel represents distances in the shortest path of the agent and the second channel represents distances from the agent's target in one of the available deviation paths. Moreover, the square submatrix highlighted in red is the agent's FOV (so the agent is in its central position) and · symbols are used to indicate absence of information.

$$\left(\begin{array}{ccc|cc} \cdot & \cdot & \cdot & \cdot & \cdot \\ \cdot & 3 & 2 & \cdot & \cdot \\ \cdot & \cdot & 1 & \cdot & \cdot \\ \cdot & \cdot & 0 & \cdot & \cdot \end{array} \right) \quad \left(\begin{array}{ccc|cc} \cdot & \cdot & \cdot & \cdot & \cdot \\ \cdot & 7 & 6 & 5 & 4 \\ \cdot & \cdot & \cdot & \cdot & 3 \\ \cdot & \cdot & 0 & 1 & 2 \end{array} \right)$$

Figure 3.5: Shortest path and one deviation path channels extracted from a 3×3 FOV in a 4×5 toy environment

In addition, the FOV observator returns an adjacency matrix A representing the current state of the environment. In particular, A would be a square matrix of dimension $n \times n$, where n is the number of agents, such that $a_{i,j} = w \neq 0$ if and only if agent i is distant $w \leq d$ from agent j . This adjacency matrix is used to record some kind of local communication network, that will be exploited by the architectures described in 6.2.2.

3.4.4 Normalization

We already mentioned that an observation should be considered as a snapshot of a state from the point of view of an agent; then we reported that this snapshot should be consistent across different runs and that it should also be shaped as a tensor of fixed size. All of this pre-preprocessing is a required step that should be carefully considered when working with neural models (the ones that will be described in subsequent chapters).

Another important aspect about neural networks is that they mostly require input features to be in comparable ranges: this can be achieved by either normalization or standardization. To be clear, the input features that we are talking about are the ones associated to elements of an observation (e.g. a node in our binary tree).

About standardization, a feature x is mapped to $x_s = \frac{x - \mu_x}{\sigma_x}$, where μ_x and σ_x are the mean and standard deviation of feature x . In this way, the resulting x_s would have zero mean and standard deviation equal to 1. One thing to notice, though, is that it requires either to know the underlying distribution of feature

x and its corresponding parameters (μ_x and σ_x) or a sample of examples from which parameters could be estimated. In the case of reinforcement learning, we definitely do not have pre-computed samples, since we work in an online fashion, meaning that observations are computed on the fly at each time-step and the network gets called with a batch of previously collected observations. Because of this, the only way in which we could standardize features would be to either know the underlying distribution of each one (which is mostly not the case), or use normalization layers in the network itself (e.g. batch normalization [8] or layer normalization [4]).

About normalization, it could be used to refer to many different things, but the main idea is again to translate an input range $[l, u]$ to a fixed output range $[min, max]$ (e.g. $[0, 1]$ or $[-1, 1]$). Usually, when the input is translated into $[0, 1]$ we talk about normalization, while when the input is translated into a range different than $[0, 1]$ we talk about min-max scaling. The general formula of min-max scaling is $x_n = l + \frac{x-min}{max-min} \cdot (u - l)$. In the more specific case of default normalization, the formula becomes $x_n = \frac{x}{max}$.

Normalization enables us to exploit domain knowledge in order to infer ranges for each feature of our observation. In particular, distances are normalized by considering a fixed observation radius as maximum and either zero or the negated radius as minimum (in the case of negative distances, which we used to indicate agents behind the given one, for example), while other features have much clearer ranges (e.g. features related to malfunctions have a minimum at 0 and a maximum at the maximum duration of a malfunction, which is a parameter of the environment).

4 Reinforcement learning setting

Introduction

In a single-agent standard reinforcement learning scenario (see figure 4.1), the problem is modeled as an MDP (Markov Decision Process), where at each discrete time-step t the agent observes the environment's state s_t (where $s_t \in S$ and S is the whole state space) and takes an action a_t (where $a_t \in A$ and A is the whole action space) that brings it to a new state s_{t+1} . Moreover, the agent receives a reward r_{t+1} proportional to the quality of taking action a_t in state s_t . Usually, rewards are local, meaning that only the given (s_t, a_t) pair should be considered when computing them. Then, the agent should learn a policy, i.e. a function $\pi : S \times A \rightarrow [0, 1]$, that maximizes the expected cumulative return, i.e. $R = \sum_{t=1}^{\infty} \gamma^t r_t$, where $\gamma \in (0, 1)$ is the discount rate (a parameter that intuitively encodes how much importance should be given to immediate or future rewards, s.t. $\gamma \rightarrow 0$ favors the former while $\gamma \rightarrow 1$ favors the latter).

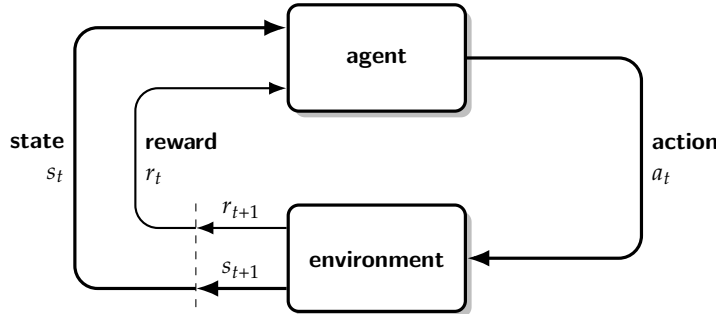


Figure 4.1: Single agent RL scenario

Since Flatland is actually a multi-agent environment, the formal definition of the reinforcement learning scenario slightly changes, but the main ideas still hold. As reported in [18], MARL (Multi-Agent Reinforcement Learning) typically represents the environment as a stochastic game. While the name is different, its fairly similar to an MDP. States become joint states of all the agents, with different rewards corresponding to each possible joint action. Transition functions remain analogous to the single-agent case, replacing states and actions accordingly.

One of the main challenges of MARL is related to non-stationary transitions, i.e. given a distinct state and action pair, the transition probabilities to other states are not constant (state transitions become dependent on the joint actions of all the agents).

Value functions

As reported in [21], almost all reinforcement learning algorithms involve estimating value functions, i.e. functions of states (or of state-action pairs) that estimate how good it is for the agent to be in a given state (or how good it is to perform a given action in a given state). The notion of how good here is defined in terms of future rewards that can be expected, or, to be precise, in terms of expected return. Of course the rewards the agent can expect to receive in the future depend on what actions it will take. Accordingly, value functions are defined with respect to particular ways of acting, called policies (which we already introduced in the previous section).

Formally, the value function of a state s under a policy π , denoted $V_\pi(s)$, is the expected return when starting in s and following π thereafter. For MDPs, we can define V_π formally by

$$V_\pi(s) = \mathbb{E}_\pi [G_t \mid s_t = s],$$

where $G_t = \sum_{k=0}^T \gamma^k r_{t+k+1}$ is the discounted return at time-step t and $E_\pi[\cdot]$ denotes the expected value of a random variable given that the agent follows policy π .

Moreover, we can also define the value of taking action a in state s under a policy π , denoted $Q_\pi(s, a)$, as the expected return starting from s , taking the action a , and thereafter following policy π :

$$Q_\pi(s, a) = \mathbb{E}_\pi [G_t \mid s_t = s, a_t = a],$$

The relationship between the V and Q functions is as follows:

$$V_\pi(s) = \sum_a \pi(s, a) \cdot Q_\pi(s, a)$$

Optimal policy

The main goal of reinforcement learning approaches is to find an optimal policy $\pi^* = \arg \max_\pi R$. To do so, different types of algorithms could be employed:

- Model-based: the agent tries to understand the world and create a model to represent it, so that, after learning, it could make predictions about what the next state and next reward will be before taking an action
- Model-free: they rely on real samples from the environment and never use generated predictions of next state and next reward to alter behaviour
 - Value-based: the policy is implicit, so that at each time-step the agent chooses the action that brings it to the next state which has the best evaluation
 - Policy-based: it avoids forming both the MDP and the value functions, and instead tries to directly learn the (optimal) policy

In this work we mainly focused on model-free, value-based techniques. Their goal is to implicitly find the optimal policy, by sequentially pushing the related value functions towards higher quality ones. In this regard, the final aim of our RL agents is to find the optimal action-value function (also called Q function), by leveraging Bellman's optimality equation:

$$Q^*(s, a) = \max_{\pi} \mathbb{E} [G_t \mid s_t = s, a_t = a, \pi]$$

4.1 Rewards and shaping

Designing rewards is a key property for the success of reinforcement learning agents. Rewards should be simple and straightforward, but they should also encode the right amount of information extracted from the domain of the application. Hence, they cannot be designed in a general fashion, because they are problem-dependent.

Flatland provides the following rewards out of the box:

- -1 for each step taken
- $+1$ when every agent arrives at their target

Training agents with the standard reward didn't seem effective in a lot of ways. For example, from our point of view it doesn't make sense to give an agent a reward of $+1$ only if all of them reached their targets. A more sensible idea would be to kind of even out all the negative rewards that the agent got during their journey to the target, but also leaving information about the number of steps that it took to arrive at the destination.

Backing the reported reasoning, the following rewards shaping was performed:

- If the agent has arrived to its target, a positive reward equal to the maximum number of steps minus the current number of steps is returned (in this way, if an agent arrives in n_1 steps in one execution and in $n_2 \leq n_1$ steps in another execution, information about the number of steps is not lost and the agent should learn to prefer the transitions that made it receive a reward of n_2)
- If the agent is in deadlock, a reward equal to the negated maximum number of steps is returned
- Because of the introduction of real decisions, rewards have to be accumulated whenever the agent is not in a decision cell (so that, for example, if an agent travels along a sequence of n straight rails, its reward would be equal to $-n$ instead of -1 when it exits the sequence)
- If an agent performed a stop action, give the agent a reward which is worse than the the reward it could have received by choosing any other action. Then, multiply this weight by the number of turns the agent consequently decided to perform a stop action and compute the product of it with a stop penalty parameter. Finally, this reward is clipped to

the maximum value given by a deadlock penalty. In this way, performing a lot of consecutive stop actions has an exponential decrease in the received rewards.

4.2 Action selection

A reinforcement learning algorithm could be considered as a search algorithm in the huge space of feasible policies. In that case, the aim of our agent would be to travel along the landscape of "policy values" in order to find the global optimum, i.e. the best policy overall. The final goal would thus be to constantly improve the current best policy, via some kind of local search, which in the case of neural networks is implemented using gradient descent.

Because of this local search perspective, another key aspect of the reinforcement learning algorithm is to balance the exploration-exploitation tradeoff. In particular, by exploration we mean probing a large portion of the search space with the hope of finding other promising solutions that are yet to be refined, while exploitation is instead related to the refinement of an already promising solution, by intensifying the search in its neighborhood.

In practical terms, at each time-step an action selector has to decide if the agent should follow the action that our current policy marks as the best one (exploitation) or choose another action (exploration), from the set of available ones.

Moreover, the farther we are in the training process of the RL algorithm the lower should be the exploration parameter, meaning that a decaying mechanism should be implemented to decrease the exploration value at each time-step. Different types of decaying methods could be implemented, like an exponential or a linear one (our experiments were conducted mostly with a linear decay, with a pre-defined number of exploration episodes).

4.2.1 ϵ -greedy

The ϵ -greedy action selector is a standard one in the RL community. It works by treating the ϵ parameter (which should be in range $[0, 1]$) as the probability of exploration, so that $1 - \epsilon$ represents the probability of exploitation.

In practical terms, given a random number $r \in [0, 1]$ sampled from a uniform distribution and the set of possible actions A , the action a_t that is selected at time t is the following:

$$a_t = \begin{cases} \max_{a \in A} Q_{\pi_t}(s_t, a) & \text{if } r \geq \epsilon \\ \text{random_choice}(A) & \text{if } r < \epsilon \end{cases},$$

where `random_choice` is a routine that samples from the given set, with a uniform distribution.

By tweaking a little bit the ϵ -greedy selector we could also get two other selectors:

- Greedy: set $\epsilon = 0$ and avoid decaying it (always select the best action)
- Random: set $\epsilon = 1$ and avoid decaying it (always select a random action)

4.2.2 Boltzmann

The Boltzmann action selector is less common in the RL community. It works by computing a modified softmax of the values associated to actions and using the resulting probability distribution to sample an available action. The balance between exploration and exploitation is controlled by the temperature parameter τ (which should be in range $(0, 1]$), so that higher values of τ will result in higher exploitation.

In practical terms, we have to model the probability of each action a_i being selected at time t with the following equation:

$$P_\tau(a_i) = \frac{\exp(Q_{\pi_t}(s_t, a_i)/\tau)}{\sum_a \exp(Q_{\pi_t}(s_t, a)/\tau)}$$

Then, a sample is drawn from the set of actions A , so that the probability of selecting action i is equal to the previously computed value $P_\tau(a_i)$.

By tweaking a little bit the Boltzmann selector we could also obtain the so-called Categorical action selector, where $\tau = 1$ and no decaying is applied to it. In this way, the probability of choosing an action is given by a default softmax over the obtained Q function values.

4.3 Action masking

One important problem that we faced while implementing our agents was related to differentiating legal and illegal moves in the learning process. In particular, in the Flatland environment the set of available choices at each time-step is strictly related to the position of the agent: for example, an agent in a straight rail can only decide to follow the path over which it is placed (so only one action would be legal), while an agent that finds itself in a fork would have more than one available actions to choose from.

Computing legal and illegal actions is not a problem in the Flatland environment, since it is fully observable, but injecting this knowledge in the reinforcement learning scheme, so that the agent can learn to avoid illegal moves, is not straightforward. A simple way to do so would be to add a penalty term in the reward, but in this way you are not completely guaranteed that agents will never select an illegal action, because that step would be part of the learning process (i.e. agents would have to learn to avoid those actions).

A more all-round solution would instead completely prevent agents to pick a move that is not available (i.e. agents should directly ignore those actions). To do so, we decided to mask out illegal moves whenever the algorithm has to do some kind of computation or selection on the set of actions. Specifically, in the action selectors we replaced every instance of the max, arg max and soft max

operator with their ad-hoc masked counterparts and we did the same when computing Bellman optimality.

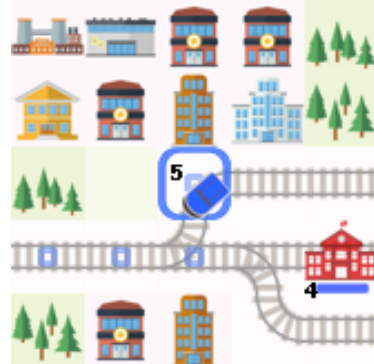


Figure 4.2: Agent with a subset of legal actions

Figure 4.2 shows an example in which the blue agent can only decide if it wants to move forward (to the join cell) or stay in its current cell (a cell before a join). Moreover, if the agent is the only one remaining in the environment, even stop moving wouldn't be a viable action to take.

5 DQN

A DQN (Deep Q -Network), as was first presented in [17], leverages neural networks from the point of view of universal function approximators, to estimate the optimal Q^* state-action function.

The main idea behind DQN is to estimate Q^* with Q_θ and use the Bellman equation to update the weights θ of the network so that $Q_\theta \rightarrow Q^*$. In particular, we will use a regression loss (e.g. MSE or Huber) like the following to minimize the so-called TD (Temporal Difference) error:

$$L(\theta) = \mathbb{E}_{(s_t, a_t, r_{t+1}, s_{t+1})} \left[\underbrace{\left(r_{t+1} + \gamma \max_{a_{t+1}} Q_\theta(s_{t+1}, a_{t+1}) - Q_\theta(s_t, a_t) \right)}_{TD}^2 \right]$$

About the network architecture, the literature does not follow a clear definition, so that the term DQN is mostly linked to the whole training pipeline required to reach good estimates of the optimal Q function. For example, in the original paper [17] DeepMind researchers use an initial CNN (Convolutional Neural Network), since their input is represented by videogame frames, followed by an MLP (Multi-Layer Perceptron). In our case, we stucked to just using the final fully-connected layers, as shown in figure 5.1, where the number of input neurons is given by the linearization of the selected observation, the number of hidden cells and the number of hidden layers are hyperparameters, while the number of outputs is equal to the size of the action space (in our case we have exactly 3 choices).

Another thing to notice is that the weights used for the target versus the current (presumably non-optimal) Q values are different. In practical terms, a separate network is used to estimate the TD target. This target network has the same architecture as the function approximator but with frozen parameters. Every T steps (a hyperparameter) the parameters from the Q -network are copied to the target network. This leads to more stable training because it keeps the target function fixed (for a while). Because of this, assuming θ to represent the current network weights and θ^- the target network weights, the loss function is updated as follows:

$$L(\theta) = \mathbb{E}_{(s_t, a_t, r_{t+1}, s_{t+1})} \left[\left(r_{t+1} + \gamma \max_{a_{t+1}} Q_{\theta^-}(s_{t+1}, a_{t+1}) - Q_\theta(s_t, a_t) \right)^2 \right]$$

There are two main ways to copy the weights from the current to the target network:

1. Hard update: every T steps, the current network is cloned into the target network

2. Soft update (or Polyak average): at every time-step a portion of the current weights is shifted onto the target ones, so that at step i we have $\theta_i^- = \tau \cdot \theta_i + (1 - \tau) \cdot \theta_i^+$, where τ is an hyperparameter that controls the weight transfer amount

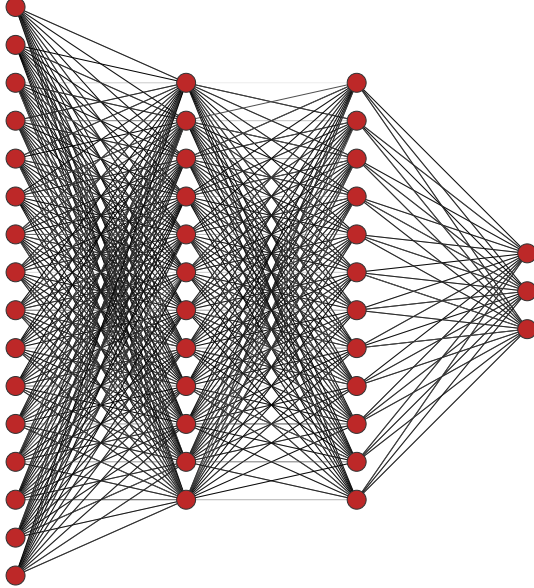


Figure 5.1: Simple DQN example with FC layers

5.1 Experience replay

We already mentioned the problem of non-stationarity related to MARL, when agents have to deal with a stochastic environment, but in practice that same problem is also present in simpler RL algorithms, since the data distribution still changes as the agent learns new behaviours (which is in contrast with the standard assumption of a fixed underlying distribution of deep learning methods). Moreover, we know that supervised learning algorithms assume samples in a dataset to be *i.i.d.* (independent and identically distributed), so that if we model the RL problem as a supervised one (e.g. a DQN can be framed as a regression problem that minimizes the distance from the optimal Q function) we break the independence assumption since sequences of states are usually highly correlated.

To alleviate the problems of correlated data and non-stationary distributions, in the original DQN formulation [17] DeepMind researchers report the use of a data structure named experience replay (also known as replay buffer in the literature), which randomly samples previous transitions, and thereby smooths the training distribution over many past behaviors. In this way, the $(s_t, a_t, r_{t+1}, s_{t+1})$ tuple shown in the previous loss equations should be considered as a sample extracted from the current replay buffer.

In practical terms, there are two main ways to implement an experience replay E :

- Uniform [17]: previous experiences are drawn from a uniform distribution $\sim U(E)$
- Prioritized [19]: authors propose to more frequently replay transitions with high expected learning progress, as measured by the magnitude of their TD error

5.2 Improvements

5.2.1 Double

One important issue of standard DQNs is that they tend to overestimate Q values (which is mostly due to the max operator in the Bellman optimality equation), leading to unstable training and low quality policies.

In order to mitigate the issue, in [7] they propose to decouple the selection of an action from its evaluation. From a practical point of view, we only have to change how the TD error is computed:

$$L(\theta) = \mathbb{E}_{(s_t, a_t, r_{t+1}, s_{t+1})} \left[\left(r_{t+1} + \gamma Q_{\theta^-}(s_{t+1}, \arg \max_{a \in A} Q_{\theta}(s_{t+1}, a)) - Q_{\theta}(s_t, a_t) \right)^2 \right]$$

Intuitively, in double DQNs we are mitigating the overestimation bias by adding a second estimator, so that chances of both estimators being overoptimistic at the same action are simply lower. In this way, estimator Q_{θ} would "obtain the best action", while Q_{θ^-} would evaluate the Q values for the estimated action, so as to average out the inherent noise.

5.2.2 Dueling

The main goal of dueling architectures, as first presented in [25], is still to solve the overestimation problem described in 5.2.1. Moreover, since for most applications it seems unnecessary to know the value of each action at every timestep, the dueling architecture can learn which states are valuable and which are not, without having to learn the effect of each action for each state.

In particular, authors rely on the fact that the Q function can be decomposed in the sum of two functions, the value function V and the advantage function A , so that $Q_{\pi}(s, a) = V_{\pi}(s) + A_{\pi}(s, a)$. Moreover, from the expression of the state-value function $V_{\pi}(s) = \mathbb{E}[Q_{\pi}(s, a)]$ it follows that $\mathbb{E}[A_{\pi}(s, a)] = 0$.

From a practical point of view, a dueling DQN can be implemented by separating the Q function estimation into two streams, the "value" and "advantage" one (as shown in the last layers in figure 5.2), to then recombine them into a single output which represents the Q estimates themselves.

The recombination layer cannot simply be the sum of the presumed "value" and "advantage" outputs, since they actually aren't reliable estimates of the mentioned functions and they suffer from lack of identifiability (meaning that, given a Q value we are not able to recover the corresponding V and A values uniquely), as thoroughly described in [25]. To this end, authors decided to force the advantage function estimator to have zero advantage at the chosen action, so that output merging could be computed by the following formula:

$$Q(s, a) = V(s) + \left(A(s, a) - \max_{a' \in A} A(s, a') \right)$$

An alternative formulation of the recombination layer is to use the average (instead of the maximum) over the advantage function. In this way, the original semantics of V and A are lost, but authors report that it eases optimization, while still preserving the relative rank of the A (and hence the Q) values. Formally:

$$Q(s, a) = V(s) + \left(A(s, a) - \frac{1}{|A|} \sum_{a' \in A} A(s, a') \right)$$

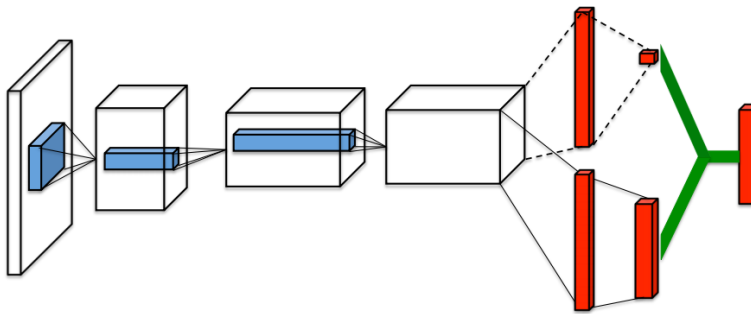


Figure 5.2: Dueling DQN architecture

5.2.3 Gradient noise reduction

Mnih et al. observed that large gradients can be detrimental to the optimization of DQNs. This was noted in the context of large reward values, but it is possible that overestimation bias can also introduce variance in the gradient and have a negative effect overall.

To solve this issue, in [17] authors decided to clip gradient values to a fairly small range (fixed to be $[-1, 1]$), while in [19] they went for a solution which clips the norm of the gradient to a specific maximum value (which was chosen to be 10).

By further inspecting the rationale behind Mnih et al. (quoted below), we can conclude that using an MSE loss and clipping gradient values to be in $[-1, 1]$ should give the same results as using an Huber loss without any kind of

gradient noise reduction. However, it's not clear if Schaul et al. followed the same reasoning.

We also found it helpful to clip the error term from the update to be between -1 and 1 . Because the absolute value loss function $|x|$ has a derivative of -1 for all negative values of x and a derivative of 1 for all positive values of x , clipping the squared error to be between -1 and 1 corresponds to using an absolute value loss function for errors outside of the $(-1, 1)$ interval. This form of error clipping further improved the stability of the algorithm.

5.2.4 Bellman operators

So far, we stucked to training the presented models with the reported losses, by having Bellman optimality in mind. As already discussed in 5.2.1 and 5.2.2, the main goal of the authors that developed the double and dueling DQN improvements was to reduce the overestimation bias of the resulting Q values, which is mainly due to the use of the max operator in Bellman's equation.

In [20], Song, Parr, and Carin explore the possibility of directly modifying Bellman's equation to understand if a change in the max operator therein could be beneficial to the Q function estimates and how this could impact their overoptimistic behavior.

In particular, other Bellman operators had already been presented, but the main two on which authors decided to focus are soft max and mellow max. The latter was first conceived in [3] to be used as either an alternative action selector (see section 4.2) or directly inside Bellman's equation. Formally, the mellow max operator can be written as

$$mm_{\omega}(s) = \frac{1}{\omega} \log \left(\frac{1}{|A|} \sum_{a' \in A} \exp(\omega \cdot Q(s, a')) \right),$$

where ω is a tuning parameter. Asadi and Littman show that mellow max converges to mean and max when $\omega \rightarrow 0$ and $\omega \rightarrow \infty$, respectively. Moreover, they also prove that mellow max is a contraction, which means that the same convergence properties guaranteed for the max operator in Bellman's equation still hold. The main disadvantage of mellow max is that it doesn't directly provide a probability distribution over actions, so that additional steps are needed to properly inject it into Bellman optimality.

About the other operator discussed in [20], it leverages a soft max modified to account for an additional temperature τ parameter (as already shown in 4.2.2), so that when $\tau \rightarrow 0$ we get back the standard Bellman equation. In practical terms, the softmax Bellman operator can be implemented by modifying how the TD error is computed, by substituting the max computation with the following formula:

$$\sum_{a_{t+1}} \frac{\exp(Q_{\theta^-}(s_{t+1}, a_{t+1})/\tau)}{\sum_{\hat{a}} \exp(Q_{\theta^-}(s_{t+1}, \hat{a})/\tau)} \cdot Q_{\theta^-}(s_{t+1}, a_{t+1})$$

Even though soft max Bellman is not a contraction (as shown in [16] with a counterexample), experiments reveal that its usage can improve test scores over standard double and dueling DQNs with certain temperature values. Moreover, authors in [20] generally observed higher maximum scores and faster learning than their max counterparts: this already suggests that the soft max operator can mitigate the overestimation bias.

However, depending upon the amount of noise, it is possible that, unlike double DQN, the reduction caused by soft max could exceed the bias introduced by max (overcompensation). But, when combined with double Q-learning, this effect becomes very small.

In our experiments, the use of the soft max Bellman operator resulted in much faster training convergence and higher test scores (see section 7.2), thus replicating the claims made in the cited paper.

6 GNN

The main goal of GNNs (Graph Neural Networks) is, given an input graph, to learn a mapping from nodes into an embedding space and use the embedded vectors to perform some kind of downstream task (e.g. node classification or link prediction).

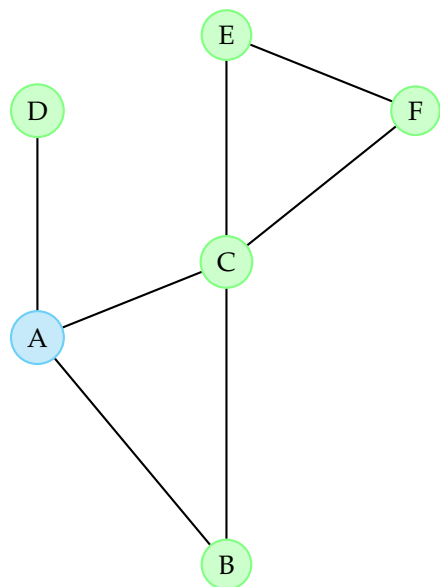
GNN architectures take inspiration from CNNs (Convolutional Neural Networks), by focusing on a local portion of the input data, thus recycling the idea of shared weights. Actually, GNNs are usually framed as a general framework that pops up more and more often in different specialized deep learning architectures: for example, the original transformer [22] designed for NLP tasks operates on fully connected graphs representing all connections between the words in a sequence (see [5] for a generalization of transformers which leverages the graph connectivity inductive bias).

Formally, given an input graph $G = (V, E)$, where V is the vertex set, E is the edges set ($E \subseteq V \times V$), we denote with A the adjacency matrix of G , so that $a_{i,j} = w \neq 0$ if and only if node i is connected to node j via the edge (i, j) that weighs w (otherwise $a_{i,j} = 0$). Moreover, we define feature matrices $X_V \in \mathbb{R}^{|V| \cdot n}$ and $X_E \in \mathbb{R}^{|E| \cdot m}$, where n is the number of features associated to each node and m is the number of features associated to each edge. Whenever features are not available for the problem at hand, simple techniques like using indicator vectors or arrays of constant values could still work, depending on the application.

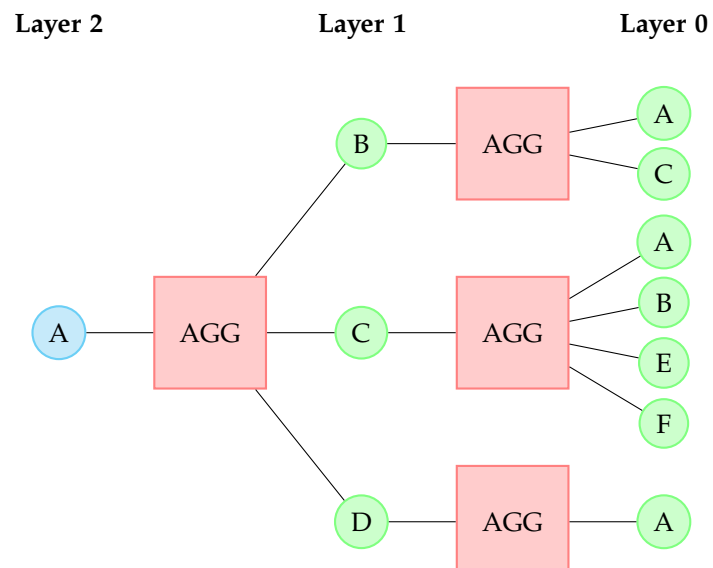
One of the key ideas in GNNs is the one referred to as message passing: nodes aggregate information from their neighbors using custom functions or function approximators. The depth at which these models operate has the following meaning:

- Layer 0: the embedding of node u is equal to its input features $X_V(u)$
- Layer 1: the embedding of node u is equal to the aggregated features $X_V(N(u))$ from its immediate neighbors $N(u)$
- Layer k : the embedding of node u is constituted by the recursive aggregation of features from nodes that are at most k hops away from u

Figure 6.1 shows an input graph and the corresponding GNN aggregations to compute an embedding for node A , with a fixed depth of 2. Key distinctions between different GNN architectures are on how different approaches aggregate information across the layers (i.e. the implementation of the AGG box in the figure).



(a) Input graph



(b) GNN aggregation

Figure 6.1: Input graph with GNN aggregation (example taken from [12])

As reported in [6], a general framework (GraphSAGE) to perform GNN aggregations (also called graph convolutions) is the following:

$$h_k(u) = \sigma([W_k \cdot f(\{h_{k-1}(v), \forall v \in N(u)\}), B_k h_{k-1}(u)]),$$

where σ is a non-linearity, W_k and B_k are trainable weight matrices for layer k , h_k is the embedding at layer k , $[\cdot]$ is the concatenation operator and the function f could be any differentiable function that maps the set of vectors in $N(u)$ to a single vector. Some examples of such functions are:

- Mean: $\sum_{v \in N(u)} \frac{h_{k-1}(v)}{|N(u)|}$
- Pool: $\gamma(\{Q \cdot h_{k-1}(v), \forall v \in N(u)\})$, where γ could be element-wise mean or max and Q is a trainable weight matrix
- LSTM: $LSTM(\{h_{k-1}(v), \forall v \in \pi(N(u))\})$, where π indicates a permutation function

GraphSAGE could also be viewed as a generalization of the previously presented GCN [11] (Graph Convolutional Network), where an embedding at layer k is computed as a simpler neighborhood average:

$$h_k(u) = \sigma \left(W_k \sum_{v \in N(u)} \frac{h_{k-1}(v)}{|N(u)|} + B_k h_{k-1}(u) \right)$$

The embeddings reported so far are only related to nodes in the graph (even though some of them also consider edge weights when computing them), but other approaches exist to directly compute edge embeddings via edge convolutions [24]. Moreover, different methods could be needed when dealing with dynamic graphs (i.e. graphs that evolve over time, both feature-wise and topology-wise).

6.1 Integrating GNNs in DQNs

In the literature, there have been lots of promising work towards the integration of GNNs and DQNs, where experiments show great generalization results over graph-structured input data.

In [2] authors study the problem of finding the optimal routing configuration for a set of traffic demands (which is NP-hard). Their solution relies on a centralized approach, where the agent has a global view of the current state and is tasked to route messages in an end-to-end fashion. In this scenario, the routing problem is defined as finding the optimal routing policy for each incoming source-destination traffic demand and the learning process is guided by an objective function that aims to maximize the traffic volume allocated in the network in the long-term. The GNN part comes into play with the state representation itself, where the graph is directly defined by the underlying network and features are attached to links between nodes (e.g. the current available capacity).

In [9], [14] and [15] authors rely on a different perspective of the input graph, which, instead of being an encoding of the input data, it's used as a form of local communication between agents. In particular, in their decentralized setting each node in the graph is an agent and the links to other agents are determined by a distance metric, so that the actual neighborhood of a node changes over time. Features are instead computed by specialized architectures (sequences of CNNs and MLPs), starting from raw local observations. In this way, both the topology of the network and the features associated to each node evolve together with the multi-agent environment, so that the overall model should be able to adapt to this dynamicity.

6.2 Architectures

6.2.1 Entire graph embeddings

Recalling the railway encoding described in 3.1, where the environment is represented as a compact graph, the observations described in 3.4 do not seem effective enough at exploiting all the underlying knowledge already encoded in the topology of the network. Up to now, the shortest/deviation paths predictor (see 3.2.1) and the binary tree observator (see 3.4.2) relied on the COJG graph only as a way to gain running time efficiency. Because of this, different experiments were made to try and extract features from the COJG graph itself.

In particular, our very first GNN attempt follows the subsequent workflow:

1. Build an observation that encodes the COJG graph and assign the following features to each node, from the point of view of one agent:
 - (a) Boolean value to indicate if the cell is free or occupied
 - (b) Distance from the agent's target
2. Associate a set of important positions to each agent:
 - (a) The position to the left of the agent, if the agent is in a decision cell
 - (b) The position to the right of the agent, if the agent is in a decision cell
 - (c) The agent's position, if in the COJG graph, otherwise its previous position in the COJG graph
3. Train agents as usual, but store graphs in the state element of the replay buffer
4. When learning, iterate over all the graphs in a batch and, for each one, compute a specified number of graph convolutions. Then, extract only the embeddings related to the previously saved important positions
5. Concatenate the extracted embeddings and use this new vector as an input for the DQN

This architecture was mainly tested in the single agent navigation round, since it didn't seem strong enough to generalize well in a multi-agent environment: in-depth results are shown in section 7.4 of the next chapter.

For future improvements, it could be interesting to see if adding more relevant features to each node in the COJG graph could boost the performance of its associated GNN, since by using the simple features listed above the model was not able to converge as expected and generalize to unseen environments.

6.2.2 Multi-agent graph embeddings

In this complex architecture we are following the same reasoning introduced in [14] and [15], where the GNN is used as a communication channel to exchange information between agents. The great thing about this architecture is that it is end-to-end differentiable, meaning that both features and actions are computed by a neural model, so that we shouldn't need all the feature engineering steps that are instead mandatory when working with simpler observations (like the tree and binary tree ones, described in sections 3.4.1 and 3.4.2, respectively).

Figure 6.2 shows the entire architecture, which in our case leverages the FOV observation (see section 3.4.3), a CNN as the encoder, a GNN as the communication framework and a DQN as the Q values estimator.

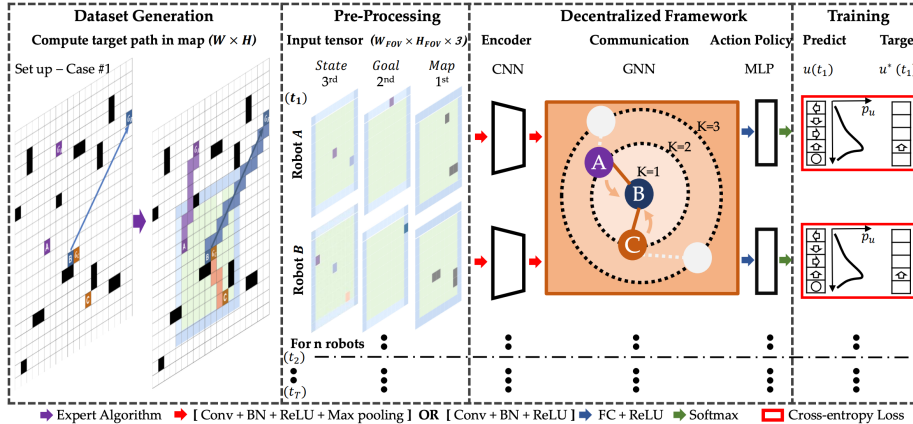


Figure 6.2: Multi-agent graph embeddings architecture (image taken from [14]).

Thanks to the FOV observator, each agent has a local Field Of View of dimension $d \times d$, where the observator's maximum depth d should be an odd number (for the reasons described in 3.4.3). First of all, the observation is fed into a CNN, built by blocks of convolution, batch normalization, activation function and (optionally) max pooling layers. The intuition behind using a CNN is that we want to enforce a local paradigm, by processing the input observation into a higher-level feature tensor.

The feature tensor produced by the CNN is then passed into a sequence of fully connected layers, so that it gets mapped to a fixed size. Then, the encoded and down-scaled observation is assigned as the feature node representing each agent in the communication graph, which encodes agent distances by edges' weights (an edge is present if and only if agents are closer than d cells). Finally, graph convolutions are performed to obtain an aggregated observation from all the neighboring agents w.r.t. a single agent (the number of executed hops is limited by a parameter).

The final aggregated information is then used as an input to the DQN, to compute the estimated Q values. Training is done by following the usual DQN pipeline, where a regression loss between the current Q function and the optimal one (according to Bellman's equation) is used to backpropagate the errors that were made during that epoch, all the way up to the initial CNN encoder.

Since this algorithm was conceived to be used in a multi-agent environment, one important modification needs to be taken into account when implementing it: an experience in the replay buffer is not related to a single agent anymore, but to all the agents in the environment.

About the specific graph filters in use in [14], authors do not give clear hints, so that we tried to implement both the simple neighborhood aggregator known as GCN [11] and a more advanced convolutional layer called GAT [23], which leverages a multi-head attention architecture.

About GAT, in its essence is just a different aggregation function with attention over features of neighbors, instead of a simple mean aggregation. The following is a description of how GAT works:

1. Compute $z_k(u) = W_k \cdot h_k(u)$, where $z_k(u)$ is a linear transformation of the lower layer embedding $h_k(u)$ and W_k is its learnable weight matrix
2. Compute $s_k(u, v) = \text{LeakyReLU}(A_k \cdot [z_k(u), z_k(v)])$, where $s_k(u, v)$ represents un-normalized attention scores between two neighbors and A_k is the additive attention weight matrix
3. Compute $a_k(u, v) = \frac{\exp(s_k(u, v))}{\sum_{w \in N(u)} \exp(s_k(u, w))}$, where $a_k(u, v)$ are the normalized attention scores on each node's incoming edges
4. Compute $h_{k+1}(u) = \sigma(\sum_{v \in N(u)} a_k(u, v) \cdot z_k(v))$, where $h_{k+1}(u)$ represents the aggregation of neighbors embeddings, scaled by the attention scores

In-depth results using both GCN and GAT layers are shown in section 7.4.

7 Results

This chapter contains a detailed description of all the experiments that were done, based on ideas that were introduced in the previous chapters. In order to present comparable results, we performed training over two types of Flatland environments, i.e. the ones identified as medium and big in table 7.1.

Parameter	Medium	Big
width	48	64
height	27	36
max_cities	5	9
max_rails_between_cities	2	5
max_rails_in_cities	3	5

Table 7.1: Test environments settings

Each environment type is then combined with a specific range of agents ([3, 5, 7] in the medium environment and [5, 7, 10] in the big one) and a complication type, which could be one of the following:

- Complication A
 - Malfunctions: absent
 - Speeds: 1.0 for each agent
- Complication B
 - Malfunctions: $\frac{1}{200} = 0.005$ rate, 15 minimum duration and 50 maximum duration
 - Speeds: 0.25 probability of having each of the speeds in $\{1, \frac{1}{2}, \frac{1}{3}, \frac{1}{4}\}$

Ideally, the training phase should span over different environments, so that agents are able to explore different samples of the same type of environment. To this end, Flatland provides a way to generate new railways out of the box, by relying on a random seed which uniquely identifies the sequence of environments that will be generated when starting from it: when training our agents, we didn't settle on a specific seed (even though seed 1 is the one we used most frequently), while when evaluating and testing them we stucked to random seed 14.

During training, models are evaluated at specific checkpoints (e.g. once every 200 training episodes), for a specified number of validation episodes (e.g. 20). A key idea about evaluation is that the model is continuosly tested over the same sequence of environments, at every checkpoint, so that we are able to observe the effectiveness of training, by looking at how agents evolve and if their behavior is getting better over time on the same set of examples.

Parameter	Description	Default value
<code>training.train_env.episodes</code>	Number of training episodes	5000
<code>env.seed</code>	Random seed to generate new railways	1
<code>env.num_trains</code>	Number of agents	-
<code>env.rewards.stop_penalty</code>	Stop penalty coefficient (see 4.1)	2.0
<code>predictor.max_depth</code>	Maximum predictor depth	-
<code>observator.max_depth</code>	Maximum observator depth	-
<code>observator.normalization_radius</code>	Maximum distance to consider in feature normalization	30
<code>learning.learning_rate</code>	Adam optimizer learning rate	$0.5e - 4$
<code>learning.tau</code>	DQN soft update weight	$1e - 3$
<code>learning.discount</code>	DQN discount factor	0.99
<code>learning.softmax_bellman.enabled</code>	Enable or disable softmax Bellman	True
<code>learning.softmax_bellman.temperature</code>	τ parameter in softmax Bellman (see 5.2.4)	0.5
<code>learning.loss</code>	Regression loss to use (Huber or MSE)	Huber
<code>action_selector.type</code>	Action selector to use (ϵ -greedy, Random, Greedy, Boltzmann or Categorical)	ϵ -greedy
<code>parameter_decay.decaying_episodes</code>	Percentage of episodes in which the exploration parameter should reach its minimum	0.7
<code>parameter_decay.start</code>	Initial exploration value	1.0
<code>parameter_decay.end</code>	Final exploration value	0.01
<code>parameter_decay.type</code>	Exploration decay type (Linear or Exponential)	Linear
<code>replay_buffer.size</code>	Replay buffer maximum size	100 000
<code>replay_buffer.batch_size</code>	Size of a batch of experiences	128
<code>replay_buffer.checkpoint</code>	How often to learn	4
DQN (model.dqn)		
<code>hidden_sizes</code>	Number and size of FC layers	[128, 128]
<code>nonlinearity</code>	Activation function (Tanh or ReLU)	Tanh
<code>double</code>	Enable or disable double DQN	True
<code>dueling.enabled</code>	Enable or disable dueling DQN	True

dueling.aggregation	Advantage function aggregation in dueling DQN (Max or Mean)	Mean
Entire graph embeddings (model.entire_gnn)		
embedding_size	Size of the output GNN embeddings	4
hidden_size	Hidden embedding size of GNN layers	8
pos_size	Number of graph embeddings to use as DQN input	3
dropout	Probability of dropout	0.2
nonlinearity	Graph convolutions activation function (Tanh or ReLU)	ReLU
Multi-agent graph embeddings (model.multi_gnn)		
cnn_encoder.conv.kernel_size	Kernel size of convolutions in the CNN encoder	3
cnn_encoder.conv.stride	Stride of convolutions in the CNN encoder	1
cnn_encoder.conv.padding	Padding of convolutions in the CNN encoder	1
cnn_encoder.pool.kernel_size	Kernel size of pooling in the CNN encoder	2
cnn_encoder.pool.stride	Stride of pooling in the CNN encoder	2
cnn_encoder.pool.padding	Padding of pooling in the CNN encoder	0
cnn_encoder.hidden_channels	Number and sizes of hidden channels in the CNN encoder	[32, 32, 64, 64]
cnn_encoder.output_channels	Number of output channels in the CNN encoder	128
mlp_compression.hidden_sizes	Number and sizes of FC layers in the MLP compressor	[]
mlp_compression.output_size	Output size of FC layers in the MLP compressor	128
gnn_communication.hidden_sizes	Number and sizes of GNN layers in the communicator	[128]
gnn_communication.embedding_size	Final embedding size in the GNN communicator	128
gnn_communication.dropout	Probability of dropout in the GNN layers	0.2
nonlinearity	Activation function (Tanh or ReLU)	ReLU

Table 7.2: Hyperparameters description

Table 7.2 contains a high-level description of all the required hyperparameters, along with their default values. Tables in the following sections will only specify those parameters that were set to a different value w.r.t. the default one.

7.1 Binary tree with DQN

Tables 7.4 and 7.5 show testing results obtained by training agents using the binary tree observator (shown in section 3.4.2) with the shortest/deviation paths predictor (shown in section 3.2.1) and a DQN model improved with all the features described in 5.2, which computes legal choices instead of actions (see 3.3.2) and aims at maximizing the expected return, where rewards are shaped as outlined in 4.1. Under the hood, both the observator and the predictor leverage the COJG graph (the one introduced in 3.1), while the environment skips unneeded computations when an agent is not in a real decision cell (see 3.3.1).

The best results were obtained when training over the medium environment with complication A, with all the hyperparameters listed in table 7.3, since agents were able to generalize in different ways: both w.r.t. the same environment type with a different random seed and with what regards another environment type (which in addition is also bigger and sparser).

Parameter	Value
env.num_trains	7
predictor.max_depth	6
observator.max_depth	6
learning.softmax_bellman.temperature	1.0

Table 7.3: Binary tree hyperparameters, trained on medium environment

Figure 7.1 reports the evolution of return (the one used for comparing test results), custom return (the one used for training the agents, described in 4.1), number of choices taken, number of elapsed turns, fraction of completions and deadlocks w.r.t. the episode number on the x -axis. As we can see, training converges to relatively high scores. Another observation is that the custom return has a much lower variance w.r.t. the standard return, which could help the stability of the DQN model. Moreover, the number of choices taken seems to remain more or less constant, independently of the decreasing value of elapsed steps as training approaches the end.

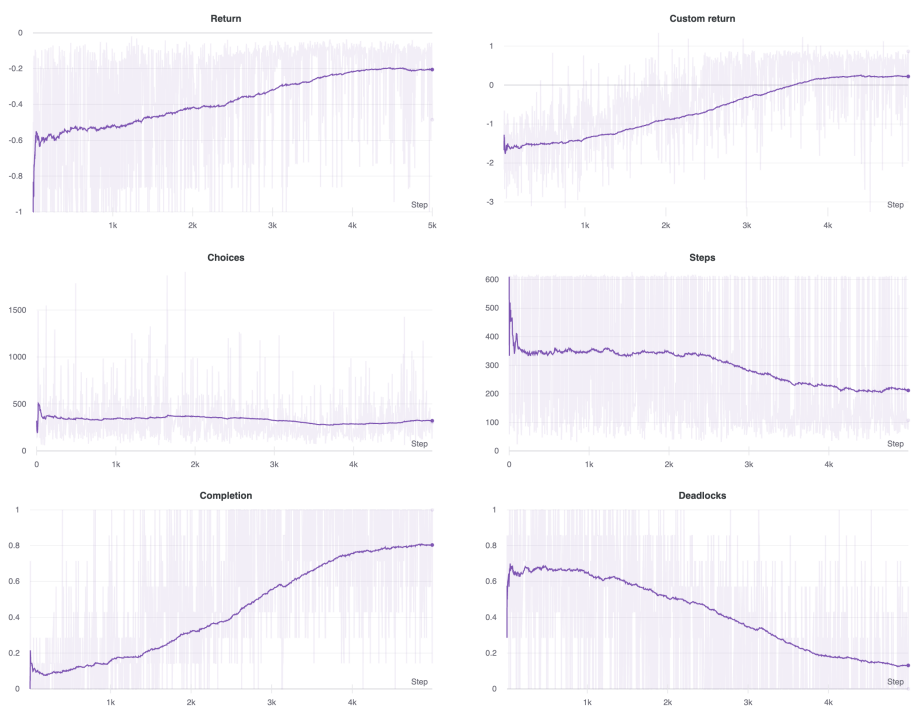


Figure 7.1: Binary tree training metrics on the medium environment

Test results show that agents behave well in differently-sized environments (i.e. the medium and the big ones), where the most difficult scenario is represented by the big environment with complication **B**. Surprisingly enough, even though agents were trained without malfunctions and with single equal speeds, they are able to adapt to both environmental complications.

	3 agents		5 agents		7 agents	
	A	B	A	B	A	B
Dones	93.07%	83.80%	89.40%	76.64%	82.51%	67.66%
Deadlocks	3.07%	5.80%	5.96%	13.40%	10.23%	12.54%
Return	-0.1404	-0.1459	-0.1581	-0.1688	-0.2057	-0.1940
Steps	142	339	187	415	250	445

Table 7.4: Binary tree results, tested on medium environment

	5 agents		7 agents		10 agents	
	A	B	A	B	A	B
Dones	86.28%	68.76%	84.17%	61.43%	76.90%	50.28%
Deadlocks	3.24%	12.88%	5.89%	20.97%	12.54%	31.82%
Return	-0.2331	-0.2081	-0.2449	-0.2260	-0.2790	-0.2615
Steps	400	637	447	650	497	675

Table 7.5: Binary tree results, tested on big environment

To conclude this section, we report other experiments that were made when training the DQN model using the binary tree observator:

1. Training over the big environment didn't work out very well: maybe, using higher depths could have helped convergence, but much more computing power was needed to perform those tests
2. Training with malfunctions and variable speeds (i.e. using complication **B**) didn't bring exciting results, but maybe training with just variable speeds could have been beneficial
3. Training without giving an increasing penalty for agents choosing to consequently take a stop moving action was detrimental: agents learned to continuously stop in order to completely avoid deadlocks
4. Training with higher hidden sizes for the FC layers in the DQN model was also ineffective: actually, we observed worse results w.r.t. using the default values reported in 7.2

7.2 Standard vs. softmax Bellman

In order to check the correctness of our softmax Bellman operator (introduced in 5.2.4) and see if we could actually observe higher test scores in the Flatland problem, we trained a DQN model using the binary tree observator (as described in 7.1), over a rather simple setting (the one specified in table 7.6).

Training was performed on the medium environment with complication A, while models were tested on the same environment type, but using a different random seed (i.e. seed 14).

Parameter	Value
training.train_env.episodes	3000
env.num_trains	2
predictor.max_depth	5
observator.max_depth	5

Table 7.6: Standard vs. softmax Bellman hyperparameters, trained on medium environment

The training results reported in figure 7.2 show that both models achieve relatively good metrics, even though the one using softmax Bellman converges much faster and to better scores than the one which makes use of the standard Bellman's equation. We can also observe much lower variances in the softmax Bellman plots.

Training results are also reflected in the test metrics shown in table 7.7, where softmax Bellman outperforms the standard Bellman operator by a good margin.

	Standard	Softmax
Dones	87.10%	89.40%
Deadlocks	6.40%	6.80%
Return	-0.1437	-0.1145
Steps	120	93

Table 7.7: Standard vs. softmax Bellman results, tested on medium environment

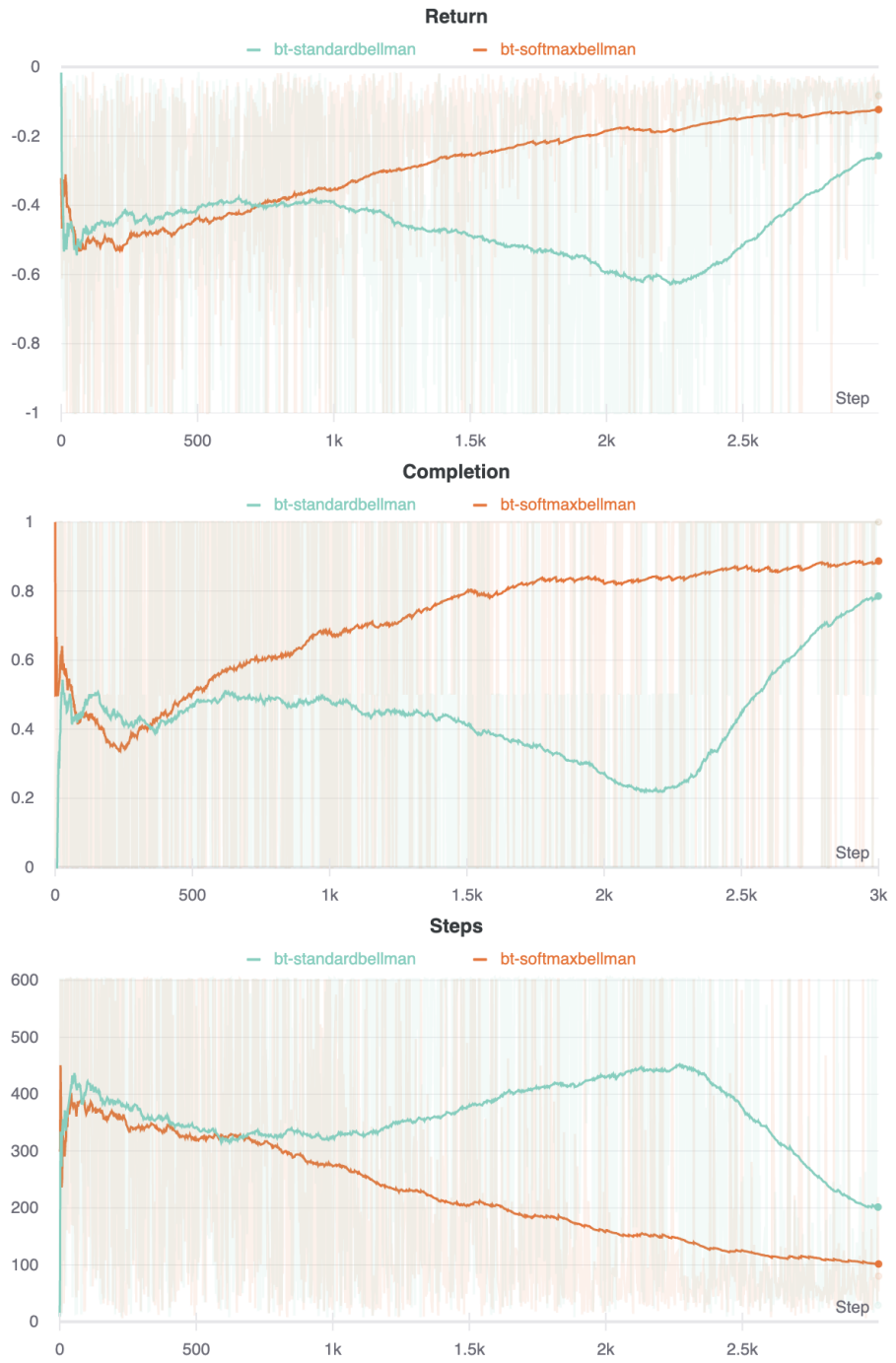


Figure 7.2: Standard vs. softmax Bellman training metrics

7.3 Comparing action selectors

This experiment aims to compare the performance of different action selectors, namely the standard ϵ -greedy and the Boltzmann ones w.r.t. random and greedy exploration baselines.

Since the DQN model using softmax Bellman in 7.2 was trained with the ϵ -greedy exploration strategy, we are going to train the same model with the Boltzmann strategy and finally observe which selector behaves the best in this particular setting. Because of this, we are keeping the same hyperparameters shown in 7.6, with the only difference being in the exploration strategy.

Figure 7.3 shows training metrics comparing bt-softmaxbellman (orange in the plots), which is the DQN model using the binary tree observator, the softmax Bellman operator and an ϵ -greedy selection strategy, and bt-softmaxbellman-boltzmann (light orange in the plots), which is the same model as the one above, with the exception of leveraging the Boltzmann action selector. Both exploration parameters (ϵ and the temperature τ) followed the same starting/ending values and decay, i.e. a linear one over a pre-defined percentage of training episodes. Moreover, the random baseline is identified by bt-softmaxbellman-randomexploration (red in the plots) and the greedy one by the term bt-softmaxbellman-greedy (blue in the plots).

Training results show that ϵ -greedy leads to faster convergence and better final scores, at least in this particular experiment.

Models were tested on the same environment type as the training one (i.e. a medium environment), but using a different random seed, as done with the previous experiments. Table 7.8 shows that testing results mirror what we observed in figure 7.3, so that the model using ϵ -greedy achieves much better scores.

	Random	Greedy	ϵ-greedy	Boltzmann
Dones	7.40%	86.10%	89.40%	84.90%
Deadlocks	28.40%	7.80%	6.80%	8.60%
Return	-0.6995	-0.1361	-0.1145	-0.1388
Steps	447	118	93	115

Table 7.8: Action selectors comparison results, tested on medium environment

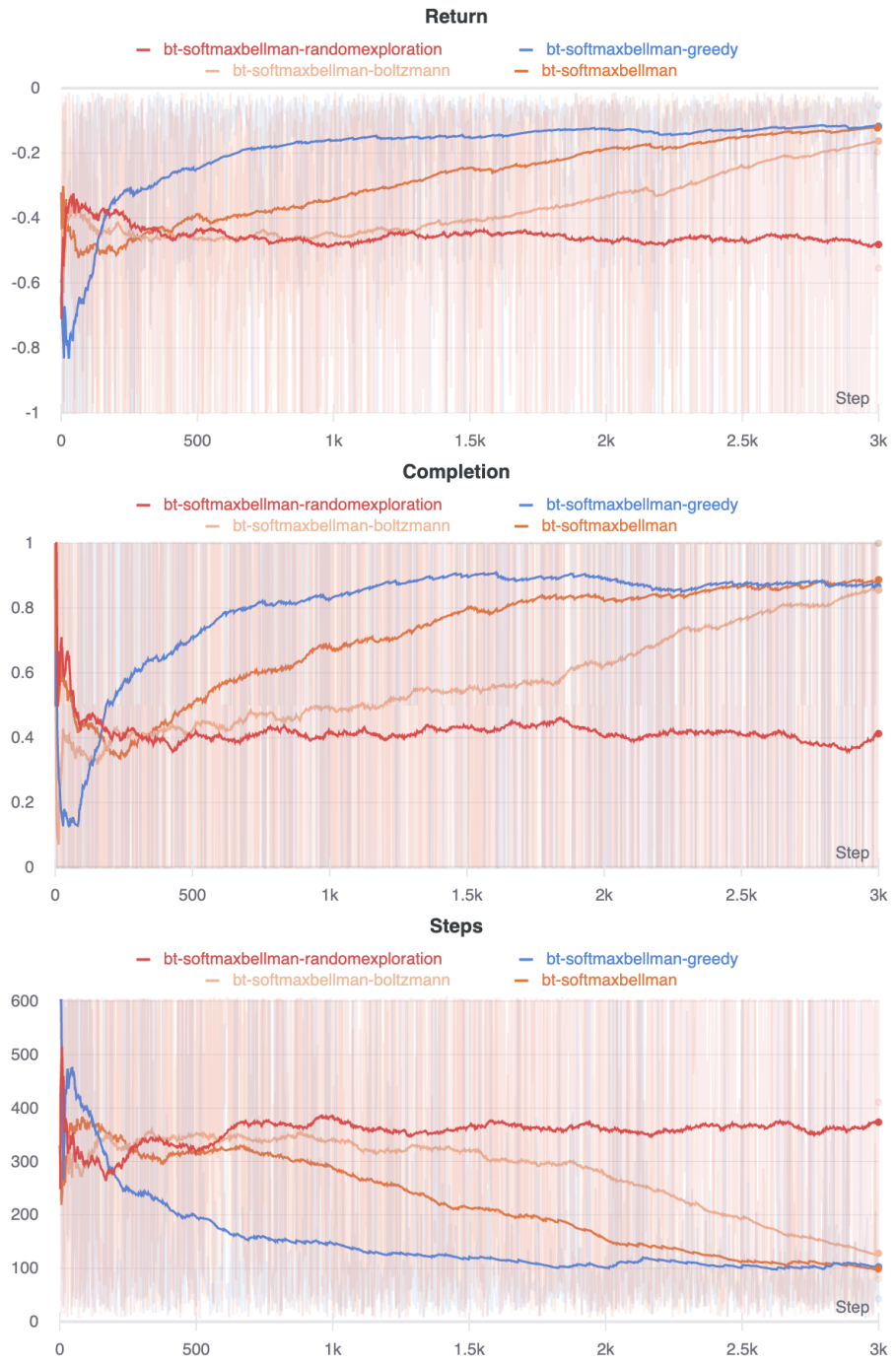


Figure 7.3: Action selectors comparison training metrics

7.4 Single-agent entire graph embeddings vs. random baseline

In this section we are reporting experiments with the model described in 6.2.1, where the COJG graph is used as the input data to a GNN model that computes node embeddings and aggregates them in a local fashion. These embeddings are then merged together and used as the state representation input in a DQN model.

As already pointed out, training was done in the medium environment with complication A and a single agent, using the parameters listed in 7.9, where the superscript indicates two different training runs. Unfortunately, training didn't converge to acceptable values, since the monitored metrics remained more or less constant throughout the entirety of executions.

Nevertheless, we tested the best obtained models using the same training settings (but with a different random seed) and compared the obtained results with a random baseline, i.e. a policy that chooses actions at random. Table 7.10 shows the outcome of such experiments.

Parameter	Value
training.train_env.episodes	3000
env.num_trains	1
predictor.max_depth	4 ⁽¹⁾ , 6 ⁽²⁾
observator.max_depth	2 ⁽¹⁾ , 6 ⁽²⁾
model.entire_gnn.embedding_size	1 ⁽¹⁾ , 4 ⁽²⁾
model.entire_gnn.hidden_size	2 ⁽¹⁾ , 8 ⁽²⁾

Table 7.9: Single-agent entire graph embeddings hyperparameters, trained on medium environment

	Random	Entire GNN (1)	Entire GNN (2)
Dones	22.80%	31.80%	53.60%
Return	-0.7947	-0.7169	-0.5160
Steps	477	433	310

Table 7.10: Single-agent entire graph embeddings vs. random baseline results, tested on medium environment

One thing that should be noticed by looking at test results is that at least the GNN model outperforms the random one by a good margin. Moreover, there seems to be a positive correlation between the size of node embeddings and final scores, which means that increasing the embedding size even further could lead to much better results.

FOV with multi-agent graph embeddings

In this final section we are reporting the achievements related to the use of the FOV observator described in [3.4.3](#), along with the neural architecture introduced in [6.2.2](#), which is a combination of the CNN, GNN and DQN models.

Following what we discovered in [7.1](#) we decided to perform very similar training runs. In particular, training was done in the medium environment with complication A and all the hyperparameter values listed in [7.11](#) (if a setting is not specified for a specific run, then it means that the default value was used).

About executions, number (1) was using the simple GCN neighborhood aggregator as the GNN filter, while the other runs were configured to use the more advanced GAT filter, described in [6.2.2](#), with 2 attention heads.

Parameter	Value
training.train_env.episodes	7500
env.num_trains	3
predictor.max_depth	$7^{(1)}, 3^{(2)}, 6^{(3)}$
observator.max_depth	$15^{(1,2)}, 27^{(3)}$
model.multi_gnn.cnn_encoder.conv.padding	$0^{(1)}$
model.multi_gnn.cnn_encoder.pool.kernel_size	$3^{(1)}$
model.multi_gnn.cnn_encoder.pool.stride	$1^{(1)}$
model.multi_gnn.cnn_encoder.hidden_channels	$[16, 32]^{(1)}$
model.multi_gnn.cnn_encoder.output_channels	$32^{(1)}$
model.multi_gnn.gnn_communication.hidden_sizes	$[]^{(1)}$
model.multi_gnn.gnn_communication.dropout	$0.0^{(1)}$

Table 7.11: Multi-agent graph embeddings hyperparameters, trained on medium environment

Models were tested on the same environment type (medium with complication A), with exactly 3 agents. Results in [7.11](#) show that increasing the model capacity, either with the use of more sophisticated layers (like the GAT one) or by increasing the size of the network, seems to reflect in higher test scores, even though final outcomes were much lower than initial expectations.

	Multi GNN (1)	Multi GNN (2)	Multi GNN (3)
Dones	18.00%	24.42%	26.13%
Deadlocks	23.33%	29.04%	37.60%
Return	-0.6631	-0.5822	-0.5194
Steps	482	433	408

Table 7.12: Multi-agent graph embeddings results, tested on medium environment

Other training trials were launched, both in a different environment type (the big one) and with an higher number of agents (i.e., 5 and 7). Again, training metrics and test results are on par with the already reported ones, so that no convergence could be reached.

From our point of view, the model that was used should be more than sufficiently capable to obtain acceptable solutions. In practice, what we observe is that training metrics remain more or less constant throughout the entire learning phase. By looking closer, it almost seems that agents are not able to understand how to reach their targets, even though the FOV observator has specific channels which encode just that information. One possible explanation to this behavior is given by the sparse setting of the Flatland environment, which does not allow to efficiently exploit local observations made out of patches extracted from the neighborhood of an agent: because of this, in our experiments we tried to enlarge the field of view each agent, reaching a quasi-global observation, but this operation didn't provide big improvements on the final scores.

Future experiments could be related to leveraging the same model described in [6.2.2](#), but using a different observation. For example, it could be interesting to try out what would happen in the following scenario:

1. Get rid of the CNN encoder and make the MLP compressor a little bit deeper
2. For each agent, use the binary tree observation (which already gives good results with a simple DQN) as the input to the MLP compressor
3. Inject the output of each call of the MLP compressor into the features of the GNN communicator's nodes (which represent agents) and perform graph convolutions, as before

In this way, agents would still exchange information locally thanks to the GNN architecture, and that information should be rich enough to converge to admissible solutions, thanks to the binary tree observation. Ideally, this architecture should outperform the standard one which uses a simple DQN and achieve better test results than the ones reported in [7.1](#).

8 Conclusions

In this work, we tested different solutions to the Flatland challenge, organized by AIcrowd [1], using both well-established techniques and cutting-edge ones.

To have a clear view of the problem, we decided to encode the environment using an efficient graph structure (i.e. the COJG graph, inspired by the COG one reported in [10] and further enhanced). This encoding was used as the basic building block for both the shortest/deviation path predictor and our custom binary tree observator, which is based on the default tree observator, but improved to have a smaller computational footprint and augmented with various findings, like real decisions and choices. Moreover, features in the binary tree are all custom-made from the ground up.

About the actual problem solution, we decided to go for a full RL setting and we adopted different models, starting from a simple DQN. First of all, we introduced various improvements in the DQN itself, like the double, dueling and softmax Bellman operators. Then, we tried to bring in further complexities, by integrating GNNs in the architecture. Our first trial with GNNs was related to encoding the entire COJG graph, performing graph convolutions directly on it and extracting pre-defined embeddings to be given as input to the DQN. The second experiment was instead related to using a different observator (the FOV one), along with a custom model comprising a CNN as the encoder of the observation, a GNN as the mean to exchange information between agents and a final DQN to compute the best actions.

Training metrics and test results show that only the improved DQN model with the binary tree observator was able to converge to acceptable solutions, while the other models containing a GNN didn't provide the outcomes we were hoping for.

Further improvements could be made to all the models and the tools we introduced, starting from the COJG graph itself. One thing that should really be tested is how to make the multi-agent graph embeddings model reach higher test scores, since the architecture itself seems a good way to go for this problem, at least from our point of view. As already reported in 7.4, the bottleneck seems to be the FOV observator, so that trying different ones could definitely boost final scores.

Flatland, and more generally MARL, is a very though problem, so that strong solutions are needed to generalize well over a wide range of environments, but we believe that research is heading in the right direction and that the integration of GNNs with standard RL models could be very beneficial.

Bibliography

- [1] Alcrowd. *Alcrowd*. URL: <https://www.aicrowd.com/>.
- [2] Paul Almasan, Jose Suarez-Varela, Arnau Badia-Sampera, Krzysztof Rusek, Pere Barlet-Ros, and Albert Cabello. *Deep Reinforcement Learning meets Graph Neural Networks: An optical network routing use case*. Oct. 2019.
- [3] Kavosh Asadi and Michael L. Littman. “A New Softmax Operator for Reinforcement Learning”. In: *CoRR* abs/1612.05628 (2016). arXiv: [1612.05628](https://arxiv.org/abs/1612.05628). URL: <http://arxiv.org/abs/1612.05628>.
- [4] Jimmy Lei Ba, Jamie Ryan Kiros, and Geoffrey E. Hinton. *Layer Normalization*. 2016. arXiv: [1607.06450 \[stat.ML\]](https://arxiv.org/abs/1607.06450).
- [5] Vijay Dwivedi and Xavier Bresson. *A Generalization of Transformer Networks to Graphs*. Dec. 2020.
- [6] William L. Hamilton, Rex Ying, and Jure Leskovec. “Inductive Representation Learning on Large Graphs”. In: *Proceedings of the 31st International Conference on Neural Information Processing Systems*. NIPS’17. Long Beach, California, USA: Curran Associates Inc., 2017, pp. 1025–1035. ISBN: 9781510860964.
- [7] Hado van Hasselt, Arthur Guez, and David Silver. “Deep Reinforcement Learning with Double Q-Learning”. In: *Proceedings of the Thirtieth AAAI Conference on Artificial Intelligence*. AAAI’16. Phoenix, Arizona: AAAI Press, 2016, pp. 2094–2100.
- [8] Sergey Ioffe and Christian Szegedy. “Batch Normalization: Accelerating Deep Network Training by Reducing Internal Covariate Shift”. In: *Proceedings of the 32nd International Conference on Machine Learning*. Ed. by Francis Bach and David Blei. Vol. 37. Proceedings of Machine Learning Research. Lille, France: PMLR, July 2015, pp. 448–456. URL: <http://proceedings.mlr.press/v37/ioffe15.html>.
- [9] Jiechuan Jiang, Chen Dun, Tiejun Huang, and Zongqing Lu. “Graph Convolutional Reinforcement Learning”. In: *International Conference on Learning Representations*. 2020. URL: <https://openreview.net/forum?id=HkxdQkSYDB>.
- [10] Wälter Jonas. “Existing and novel Approaches to the Vehicle Rescheduling Problem (VRSP)”. MA thesis. HSR Hochschule für Technik Rapperswil, Mar. 2020.
- [11] Thomas N Kipf and Max Welling. “Semi-Supervised Classification with Graph Convolutional Networks”. In: *arXiv preprint arXiv:1609.02907* (2016).
- [12] Srijan Kumar. *CSE 6240: Web Search and Text Mining*. University lecture. 2020. URL: <https://cs.stanford.edu/~srijan/teaching/cse6240/spring2020/>.

- [13] Jing-Quan Li, Pitu B. Mirchandani, and Denis Borenstein. "The vehicle rescheduling problem: Model and algorithms". In: *Networks* 50.3 (2007), pp. 211–229. doi: <https://doi.org/10.1002/net.20199>.
- [14] Qingbiao Li, Fernando Gama, Alejandro Ribeiro, and Amanda Prorok. "Graph Neural Networks for Decentralized Multi-Robot Path Planning". In: *arXiv preprint arXiv:1912.06095* (2019).
- [15] Qingbiao Li, Weizhe Lin, Zhe Liu, and Amanda Prorok. *Message-Aware Graph Attention Networks for Large-Scale Multi-Robot Path Planning*. 2020. arXiv: [2011.13219 \[cs.RO\]](2011.13219).
- [16] Michael Lederman Littman. "Algorithms for Sequential Decision-Making". AAI9709069. PhD thesis. USA, 1996. ISBN: 0591163500.
- [17] Volodymyr Mnih, Koray Kavukcuoglu, David Silver, Alex Graves, Ioannis Antonoglou, Daan Wierstra, and Martin Riedmiller. "Playing Atari with Deep Reinforcement Learning". In: (2013). cite arxiv:1312.5602Comment: NIPS Deep Learning Workshop 2013. url: <http://arxiv.org/abs/1312.5602>.
- [18] Austin Nguyen. *Multi-Agent Reinforcement Learning: The Gist*. URL: <https://medium.com/swlh/the-gist-multi-agent-reinforcement-learning-767b367b395f>.
- [19] Tom Schaul, John Quan, Ioannis Antonoglou, and David Silver. *Prioritized Experience Replay*. cite arxiv:1511.05952Comment: Published at ICLR 2016. 2015. url: <http://arxiv.org/abs/1511.05952>.
- [20] Z. Song, R. Parr, and L. Carin. "Revisiting the Softmax Bellman Operator: New Benefits and New Perspective". In: *ICML*. 2019.
- [21] Richard S. Sutton and Andrew G. Barto. *Reinforcement Learning: An Introduction*. Second. The MIT Press, 2018. url: <http://incompleteideas.net/book/the-book-2nd.html>.
- [22] Ashish Vaswani, Noam Shazeer, Niki Parmar, Jakob Uszkoreit, Llion Jones, Aidan N. Gomez, Łukasz Kaiser, and Illia Polosukhin. "Attention is All You Need". In: 2017. url: <https://arxiv.org/pdf/1706.03762.pdf>.
- [23] Petar Veličković, Guillem Cucurull, Arantxa Casanova, Adriana Romero, Pietro Liò, and Yoshua Bengio. "Graph Attention Networks". In: *International Conference on Learning Representations*. 2018. url: <https://openreview.net/forum?id=rJXMpikCZ>.
- [24] Yue Wang, Yongbin Sun, Ziwei Liu, Sanjay E. Sarma, Michael M. Bronstein, and Justin M. Solomon. "Dynamic Graph CNN for Learning on Point Clouds". In: *ACM Trans. Graph.* 38.5 (Oct. 2019). issn: 0730-0301. doi: <10.1145/3326362>. url: <https://doi.org/10.1145/3326362>.
- [25] Ziyu Wang, Tom Schaul, Matteo Hessel, Hado Van Hasselt, Marc Lanctot, and Nando De Freitas. "Dueling Network Architectures for Deep Reinforcement Learning". In: *Proceedings of the 33rd International Conference on International Conference on Machine Learning - Volume 48*. ICML'16. New York, NY, USA: JMLR.org, 2016, pp. 1995–2003.